Quantification of Residual Stresses in Electron Beam Welded Fracture Mechanics Specimens

Quantification of Residual Stresses in Electron Beam Welded Fracture Mechanics Specimens

Authors: Priyesh Kapadia[1], Catrin Davies[1], Thilo Pirling[2], Michael Hofmann[3], Robert Wimpory[4], Foroogh Hosseinzadeh[5], David Dean[6], Kamran Nikbin[1]

1. Department of Mechanical Engineering, Imperial College London, South Kensington Campus, London, SW7 2AZ, UK
2. Institut Max von Laue-Paul Langevin, 6 rue Jules Horowitz, BP156, F-38042 Grenoble, France
3. Heinz Maier-Leibnitz Zentrum (MLZ), Technische Universität München, Lichtenbergstr. 1., D-85747 Garching, Germany
4. Helmholtz-Zentrum Berlin, Hahn-Meitner-Platz 1, D-14109 Berlin, Germany
5. The Open University, Materials Engineering, Walton Hall, Milton Keynes, MK7 6AA, UK
6. EDF Energy Nuclear Generation, Barnett Way, Barnwood, Gloucester, GL4 3RS. UK.

Abstract

Residual stress measurements have been made in a range of electron beam welded samples to study how the weld induced residual stresses redistributed during fabrication of compact tension, C(T), specimens. The samples were manufactured from Type 316H stainless steel in the ex-service material condition and in material which had been preconditioned by inducing 8% plastic strain. Measurements made using neutron diffraction, slitting and the contour method were generally in good agreement and showed residual stress components of up to three times the base material's yield strength existed in the samples. When sectioning a sample to perform the contour method, large elastic deformations occurred at the cut tip due to the large residual stresses present. A correction was applied to the measured surface displacements to account for this deformation. Neutron diffraction measurements were made at various stages of the fabrication process, which showed significant stress redistribution occurred as the welded samples were machined into C(T) specimens. However the tensile stresses near the crack tip of the C(T) specimens remained large and could significantly influence subsequent crack growth tests.

Highlights

- Electron beam welding is shown to produce repeatable residual stress fields in thick samples

- Longitudinal stress components of up to three times the base material's yield stress were measured
- The residual stresses measured by neutron diffraction, the contour method and slitting techniques are in good agreement
- A correction was applied to the contour method measurements to reduce the error due to cut tip deformations

1 Introduction

Electron beam (EB) welding can create welds with large penetration depths whilst introducing fusion zones which are substantially narrower than conventional welding techniques, therefore this process is suitable for welding thick samples. During EB welding, the kinetic energy of a beam of electrons is transferred to two mating surfaces of a component as heat, which causes fusion of the material. No filler metal is used for this welding process. Large plastic deformations occur in the fusion zone and surrounding heat affected zones (HAZ). Therefore a strain misfit is created between such regions and the parent material. As a result, residual stresses are induced near the weld.

Power plants, such as the UK's advanced gas-cooled reactor plant, contain components fabricated using conventional welding techniques that have not been post weld heat treated (Coleman et al., 1998). During service at high temperatures, cracking has occurred near weld regions where the residual stresses contributed to the crack driving force exerted. These stresses need to be taken into account when making crack growth predictions to estimate the service life of components. In recent studies, EB welding has been used to fabricate fracture mechanics specimens with the purpose of conserving ex-service weld material when making large test specimens (Davies et al., 2010) or investigating the effects of residual stresses on creep crack growth (CCG). Some of the EB welded C(T) specimens presented in this work were creep tested at 550°C for up to 1,300 h under secondary and combined loading conditions and crack growth of up to 3.3 mm was observed (Kapadia et al., 2015).

The aim of this study was to investigate the magnitude of residual stresses induced in EB welded C(T) specimens. A review of neutron diffraction (ND) measurements for six

EB welded C(T) specimens, which have undergone different fabrication processes, is presented to compare the magnitude of residual stresses induced. Measurements were made at various stages during fabrication, which enabled the residual stresses induced following welding and their redistribution during subsequent machining of the samples to be quantified. Measurements were made using the instruments SALSA, Stress-Spec and E3 at the ILL, FRM-II and HZB research facilities respectively. The contour method and slitting were performed on one of the specimens to allow comparison with ND measurements. Quantification of the residual stresses in the present work enables the crack driving force to be estimated using assessment procedures such as the R5 high temperature structural integrity procedure (EDF Energy, 2014).

In the following section the designs of the specimens tested are described. Section 3 presents an overview of each of the residual stress measurement techniques and details of the experimental procedures. The measurement results and discussion are presented in Sections 4 and 5 respectively.

2 Specimen Designs

EB welds were made in blocks of ex-service Type 316H austenitic stainless steel. All of the blocks were sized to fabricate C(T) specimens with a thickness, B, of 25 mm and a width of W = 50 mm in accordance with the ASTM 1457-13 testing standard (ASTM, 2013). The configurations of the various samples tested are shown in Figure 1. Initially the weld samples included sacrificial material to contain the start, end and root of the EB weld, as shown in Figure 1(a) and (b). These sacrificial blocks were then removed by wire electrical discharge machining (EDM) to create C(T) blanks which had dimensions of 62.5 × 60.0 × 25.0 mm^3, as shown in Figure 1(c) and (e). Following this, notches were inserted into the C(T) blanks by wire EDM to fabricate C(T) specimens, as shown in Figure 1(d) and (f). The orientation of the notches were such that the longitudinal residual stresses from the EB welds were in the normal direction to the specimen's crack plane.

Table 1 presents the list of specimens measured using the ND technique. In EB1 and EB2, the EB welds were made adjacent to manual metal arc (MMA) welds to fabricate

C(T) specimens with the EDM notches located in the HAZ from the MMA welds. In these specimens the EB welds were used to attach extension arms, made from Type 316H parent material, to the C(T) specimens to conserve the ex-service MMA weld metal (Davies et al., 2010). Residual stress measurements were made in specimen EB1 in the C(T) blank configuration and in EB2 which was tested after pin holes and notches were machined using wire EDM. Two configurations of EB2 were tested with notch lengths (a/W) of 0.50 and 0.57 and are identified as EB2 EDM1 and EB2 EDM2 respectively.

C(T) specimens EBW1, EBW3, EBW4 and EBW5 were made from parent material from an ex-service steam header component, i.e. no MMA welds were present in these specimens. Residual stress measurements were made at various stages of fabrication, i.e. after welding, after removal of the sacrificial material to create C(T) blanks and as C(T) specimens, as shown in Table 1. These consecutive measurements enabled the redistribution of the weld residual stresses to be assessed. In EBW3 and EBW5 an EDM notch was located in the C(T) specimen such that the a/W ratio was 0.44. Specimens EBW1, EBW3 and EBW4 were made from ex-service Type 316H stainless steel in the as-received condition whilst EBW5 was made from ex-service material which had been additionally cold worked. Blocks were uniformly compressed at room temperature to generate 8% plastic strain. The plastic strains induced during this preconditioning process reduced the creep ductility of the material which made it suitable for performing short term CCG tests (Mehmanparast et al., 2013). The material was compressed in the direction normal to the C(T) specimen's crack plane, i.e. the y direction in Figure 1. Tensile curves for Type 316H stainless steel in the ex-service and pre-compressed material conditions at room temperature are shown in Figure 2. Specimen EBW1 was welded with a beam power and with weld speeds of 12.0 kW and 3.3 mm/s respectively. Specimens EBW3, EBW4 and EBW5 were welded with beam powers of 5.7 kW and with weld speeds of 6.3 mm/s. Due to the large heat input in EBW1, a wide weld was produced with a width of 4 mm. The beam parameters were optimised to create a narrow weld for specimens EBW3, EBW4 and EBW5, where the weld width was 1 mm. Specimen EBW4 experienced two weld cycles, where the EB was traversed across the weld line twice. The ND measurements were used to

determine whether the second weld would increase the residual stresses in comparison to EBW3 which had one weld.

3 Residual Stress Measurements

3.1 Overview

Various measurement techniques are available to quantify residual stresses in specimens and components. Non-destructive methods include neutron and X-ray diffraction, where the atomic spacing of the material is used as a strain gauge. Destructive techniques include hole drilling, slitting and the contour method. In such methods residual stresses are inferred from distortions or relaxed strains caused by stress redistribution following cutting of the sample. The number of stress components that can be evaluated vary between each technique. There are also limitations to the size of the sample and spatial resolution of the measurement region for each measurement method. The ND, contour method and slitting techniques were used in this study to measure residual stresses in EB welded specimens and are detailed in this section.

3.2 Neutron Diffraction

The ND measurement technique is a non-destructive method for evaluating residual strains in polycrystalline materials. The spacing between planes of atoms in a material, d, is determined by measuring the diffraction angle of an incident neutron beam. The experimental set up is shown in Figure 3. Residual stresses cause changes in the lattice spacing. Comparison of the diffraction angle, θ, caused by the stressed component and that of a stress free sample, using Equation (1), allows the residual strains to be determined.

$$\varepsilon_{hkl} = \frac{d_{hkl} - d_{0,hkl}}{d_{0,hkl}} = \frac{sin\theta_{0,hkl}}{sin\theta_{hkl}} - 1 \quad (1)$$

where ε_{hkl} is the lattice strain of the $\{hkl\}$ crystallographic plane, $d_{0,hkl}$ is the reference lattice spacing and $\theta_{0,hkl}$ is the reference scattering angle which are measured from a strain free sample. Residual stresses may be calculated providing the strains have been measured in three mutually orthogonal directions using:

$$\sigma_i = \frac{E_{hkl}}{1+\nu_{hkl}}\varepsilon_i + \frac{\nu_{hkl}E_{hkl}}{(1+\nu_{hkl})(1-2\nu_{khl})}(\varepsilon_1+\varepsilon_2+\varepsilon_3) \quad (2)$$

where E_{hkl} and ν_{hkl} are Young's modulus and Poisson's ratio respectively of the $\{hkl\}$ crystallographic plane. For Type 316H austenitic stainless steel, these constants for the $\{311\}$ plane are 183.5 GPa and 0.31 respectively, as determined by the Kröner model (Hutchings et al., 2005).

The gauge volume of the measurement is defined by the cross sections of the incident and diffracted neutron beams, as shown in Figure 3. At each measurement location, the number of neutrons measured across a small range of scattering angles by the detector is fitted to a Gaussian distribution and each location is sampled until a sufficient number of neutrons are detected to determine θ. The sampling time is dependent on the grain size of the material, the neutron flux of the incident beam, the gauge volume size and the path length of the beam inside the specimen (Holden, 2013). The uncertainty in fitting the Gaussian profile is used to determine the error in residual strain and stress measurements.

In the EB welded specimens residual strains were measured using the ND measurement technique in three orthogonal directions, which were in the longitudinal, transverse and normal directions to the weld. It was assumed that these orientations were aligned to the directions of the principal strains, which allowed the stresses to be determined using Equation (2) (Hutchings et al., 2005). Residual strain measurements on a similar specimen in eight directions were performed by Traore et al. (2013) to show that the principal stress components were closely aligned to the specimen's axes. The measurement lines for each of the EB welded specimens are shown in Figure 4. Measurements were made along scan lines which extended across the EB weld and were located at mid-thickness and at mid-length of the specimens. In the C(T) specimens, the measurement lines were located in the notch planes. In specimens EB1 and EB2 the measurement lines were located in the HAZ of the MMA weld. In the C(T) specimen configuration of EBW5, measurements were additionally made at quarter thickness (line EE) of the specimen to assess the through thickness variation of residual stresses.

Measurements were made using three instruments: SALSA at the ILL, Grenoble (Pirling et al., 2006), Stress-Spec at FRM II, Munich (Hofmann et al., 2006) and E3 at HZB, Berlin (Boin et al., 2014). All of these instruments are monochromatic beam diffractometers which use constant wavelength neutron beams. Due to this, the diffraction of only one $\{hkl\}$ plane was measured. Strains were measured in the $\{311\}$ plane as the elastic response for this plane in austenitic stainless steels can be assumed to remain linear at large applied stresses (Hutchings et al., 2005). Gauge volumes of $2 \times 2 \times 2$ mm^3 were used for all the specimens measured using the instruments SALSA and Stress-Spec and specimen EBW1 measured using E3. This size sampled a sufficient number of grains permitting reasonably low count times, of up to 30 min/point for SALSA and Stress-Spec and 45 - 60 min/point for E3 measurements. This gauge volume was small enough to approximate the strain measurements to point locations. However, the neutron incident beam on E3 had less intensity when measuring specimen EBW4 and therefore the gauge volume used was $2 \times 2 \times 10$ mm^3 to ensure reasonably low count times, of up to 60 min/point. As a result the strains were measured over a relatively larger region within the specimen. The material had relatively large grains, which were measured to be 80 - 120 μm in specimens EBW3, EBW5, EBW6 and EBW7 (Kapadia et al., 2015), and therefore all the specimens were oscillated by up to ± 2.4° to increase the number of grains sampled.

Reference scattering angles must be measured at stress free locations. Welding causes microstructural and chemical composition changes to the material which could cause variations in these reference measurements. Ideally reference strain measurements are made on small cube or matchstick coupons extracted from various regions across the specimen, as the residual stresses are relieved during machining of these coupons. However where the specimen could not be sectioned to extract such coupons the far field approach recommended by Withers et al. (2007) may be used. In this approach a region far from the weld and near the specimen's surface is assumed to be stress free. In EBW1 a small coupon was extracted from the ex-service component that was representative of the parent material. A toothcomb specimen was extracted from EBW4 to assess the variation of the reference strain measurements

across the weld, as shown in Figure 5. The cross sectional area of the tooth was 1.1 × 3.0 mm^2. A small tooth width was chosen to allow reference measurements to be taken exclusively in the fusion and the HAZ regions. Measurements in this toothcomb sample were made using the instrument Stress-Spec at FRM-II using a gauge volume of 0.5 × 2.0 × 10.0 mm^3. The toothcomb sample was accurately positioned using a theodolite telescope, ensuring the measurement gauge volume was in the centre of each tooth. Additionally in EBW3, EBW4 and EBW5, reference measurements were made on the corner of the specimen in the parent material which was considered to be stress free. In specimen EB1 reference measurements were made near the face of the specimen across the EB weld, as shown by line FF in Figure 4(e). In EB2, a 4 mm thick slice of material was extracted from one end of specimen and used to make reference measurements, as shown by line II in Figure 4(f) (Davies et al., 2010).

3.3 Slitting

The slitting technique experimentally determines the stress intensity factor, K, and a single component of residual stress in the component being measured. A sample containing residual stresses is incrementally cut using wire EDM. Strain relaxation is measured using strain gauges usually located at the back face of the cut profile (Hill, 2013; Prime, 1999), as shown in Figure 6.

The stress intensity factor, K, is calculated from back face relaxed strains using:

$$K(a) = \frac{E'}{Z(a)} \frac{d\varepsilon}{da} \tag{3}$$

where ε is the back face relaxed strain, a is the crack length, i.e. cut distance, E', is the plane stress or plane strain Young's modulus and $Z(a)$ is the influence function which is dependent on the geometry and strain measurement location. Schindler and Bertschinger (1997) present analytical expressions for $Z(a)$ for a rectangular plate, which the C(T) blank can be approximated to.

The residual stresses are calculated using a geometry dependent expression that relates K to an arbitrary loading condition for the same mode of fracture. This weight function solution for a C(T) specimen is (Fett and Munz, 1997):

$$K(a_i) = \sum_{j=1}^{i} \sigma_j \int_{a_{j-1}}^{a_j} h(x, a_i)\ dx \tag{4}$$

where the expression for $h(x, a_i)$ is presented by Fett and Munz (1997). The integral of $h(x, a_i)$ in Equation (4) was solved with Gaussian integration over i intervals, where i is the number of strain measurements taken during the cut process. Using Equation (3) and by assuming σ is constant over each interval, the stress profile can be determined. This approach is consistent with that presented by Prime (1999).

The slitting method was performed on specimen EBW4 in the C(T) blank configuration. The cut plane is shown in Figure 6 which is the transverse – normal (x–z) plane to the weld. Therefore, a line profile distribution of the longitudinal stress component that is averaged through the thickness of the specimen was determined.

Three strain gauges (type KFG-02-120-C1-11L5M3R) with a gauge length of 0.2 mm were mounted on the back face of the specimen at mid-thickness and quarter thicknesses as shown in Figure 6. The gauges were encapsulated with the transparent silicon potting compound QSil 12 to ensure they remained waterproof whilst submerged in water during cutting.

Cutting was performed by wire EDM, using a wire diameter of 0.25 mm whilst submerged in de-ionised water. Strain measurements were made at incremental cut distances of 0.3 mm. All measurements were made after the power to the EDM wire was stopped and the tank had been drained of water such that the specimen was in air. The strains were recorded after the readings stabilised to within 1 - 2 $\mu\epsilon$. Usually for the slitting method the sample is not cut in two parts; one side of the sample is clamped and the other side is left free hanging out in the EDM tank. However, in this research the contour and slitting methods were conducted in tandem. The sample had to be cut in two halves in order to measure the surface deformation of the created cut surfaces for the contour method. The recommended clamping strategies for the

contour and slitting methods are different. Therefore, a compromise had to be made regarding clamping the sample under consideration. One side of the specimen was clamped allowing half of the component to deform during cutting. A bar was placed underneath the free side of the specimen to prevent it from falling following the cut (see Figure 7). The cut was visually inspected by eye throughout to ensure mouth closure did not occur which would invalidate the slitting technique.

3.4 The Contour Method

The contour method is a destructive strain relief technique for two dimensional (2D) measurement of residual stress over the plane of interest (Prime and DeWald, 2013). Unlike scattering techniques such as ND, the contour method is not sensitive to microstructural variation and in theory is not limited by the geometrical complexity or size of the component being measured. The implementation of the technique involves sectioning the component in two symmetric halves using wire EDM. The deformation of the cut surfaces caused by stress relaxation is experimentally measured. The measured surface deformations are applied as a surface boundary condition in a corresponding finite element (FE) model of the cut part to back calculate the residual stresses using an elastic stress analysis. By extension of Bueckner's superposition principle (Bueckner, 1958) these stresses must be equivalent to the residual stresses that existed in the original sample prior to cutting.

The slitting and contour method measurements were applied in tandem on EBW4 specimen to measure the longitudinal stress. On completion of the slitting method measurement on EBW4, the sample was severed in two parts to measure the cut surface profiles for the contour method.

The profiles of the deformed cut surfaces were determined using a measurement procedure consistent with that reported by Traore et al. (2013). A Mitutoyo Crysta Plus 574 co-ordinate measuring machine (CMM) equipped with a 3 mm diameter Renishaw PH10M touch trigger probe was used. Measurements were made in a 0.5 × 0.5 mm^2 grid and the profiles of the perimeter of the cut parts were traced. The two data sets were averaged to remove anti-symmetric errors (due to shear stress or cutting artefacts) and the data was smoothed to prevent any noise in the data causing

localised stress peaks in the subsequent FE analysis. Cubic splines were fitted to the data. The optimum knot spacing was selected by calculating stresses for spacings of 1 mm, 2 mm, 3 mm, 4 mm, 5 mm, and 6 mm. An error was determined by comparison of the stress at each node to that of a coarser spacing, following the methodology detailed by Prime et al. (2004).

A three dimensional (3D) FE model of half of the C(T) blank was created using the FE software ABAQUS (2011). The cut face was meshed with 0.50 × 0.50 × 0.15 mm^3 elements with the mesh swept to the opposite face with increasingly longer elements up to a size of 0.50 × 0.50 × 4.00 mm^3. The model had 108,000 quadratic hexahedral elements (type C3D20R) and 459,557 nodes. The analysis was also performed using a model with 1.00 × 1.00 × 0.15 mm^3 sized elements at the cut face to determine the mesh sensitivity of the results. The processed deformation data were applied as displacement boundary conditions on the cut face. A linear elastic material model was used with Young's modulus, E, and Poisson's ratio, ν, of 205 GPa and 0.29 respectively (Mehmanparast et al., 2016) to determine the residual stresses that existed before sectioning the sample.

For the slitting method, it was required to cut the sample incrementally and clamp only one side of the specimen during cutting. Incremental cutting could cause local cutting irregularities on the surface that could lead to errors in the contour method results. Although anti-symmetric surface features due to incremental cutting are cancelled in the averaging step of the data processing, this effect was minimised by using low power wire EDM cut settings (Prime and DeWald, 2013; Prime and Kastengren, 2011). The clamping arrangement of the specimen was not ideal for the contour method measurement. The contour method requires clamping of both sides of the specimen securely and symmetrically about the cut plane, to prevent movement of the component as stresses relax during cutting. In addition secure and symmetrical clamping reduces cutting induced plasticity and reduces the elastic cut tip deformation error, which is called the "bulge error" (Prime et al., 2004; Prime and DeWald, 2013). Cutting induced plasticity violates the assumption of the contour method that the stress relaxation process is entirely elastic. The cut tip deformation violates the assumption that a constant width of material is removed by the cutting process.

An iterative FE procedure has been developed by Prime and Kastengren (2011) to correct for the bulge error. This correction procedure is implemented on the contour method results of the EBW4 specimen. The initial estimate of the residual stresses were transferred to a full 3D model of the C(T) blank and the EDM cutting process was simulated by incrementally removing elements. From this simulation the displacements associated with cut tip opening or closure were determined, and a correction was applied to the experimentally measured deformations. This iterative procedure was repeated until the obtained residual stress field using the corrected deformations converged.

4 Results

4.1 Neutron Diffraction

Measurements were made in stress free samples to determine the reference scattering angle, $2\theta_0$. The microstructure of a sectioned EB weld, presented in Figure 8(a), shows the weld and HAZ regions were approximately 1 mm wide. The effect of this variation in microstructure on $2\theta_0$ was investigated. Reference measurements of the diffraction angle made on samples assumed to be stress free are shown in Figure 8(b) and Figure 9. Reference measurements were made across lines FF and II in specimen EB1 and the sliced coupon from EB2 respectively, using a $2 \times 2 \times 2$ mm^3 gauge volume, which are shown in Figure 9. The data points at 0 mm correspond to the centre of the EB weld whilst the data points at positive distances are measurements in the MMA weld. In Figure 8(b) and Figure 9, the scattering angles have been normalised using Equation (1) where a far field scattering angle measurement is used as a reference value. The scattering angles are presented as micro-strain ($\mu\epsilon$). In EB1 a large variation in scattering angle was observed across the EB weld in all three directions, hence these measurements do not appear to have been made in a stress free region. Measurements in EB2 were made in a 4 mm thick slice removed near one end of the C(T) blank. The scattering angle magnitude was generally constant in the parent material up to the EB weld, whilst large variations were observed in the MMA weld and HAZ regions. Reference measurements made across the toothcomb sample from EBW4 in the longitudinal (y) and transverse (x) directions are shown in Figure 8(b). These measurements were made using the instrument Stress-Spec at

FRM II with a small gauge volume of 0.5 × 2 × 10 mm^3 as the sample had teeth with cross sectional areas of 1.1 × 3.0 mm^2. The centre tooth consisted of the EB weld only and therefore one measurement was made exclusively in the weld region. The measurements either side of the centre tooth were in the HAZ of the EB weld with the teeth further away in the parent material. The scattering angle in the transverse direction was marginally lower near the weld region however it was difficult to distinguish this trend from scatter in the data.

A systematic variation of lattice spacing across the EB weld was not observed in the toothcomb specimen from EBW4 or in the slice from EB2 in the parent material up to the EB weld. A change in the lattice parameter can be caused by a change in composition of the material, which can occur during welding. Whilst the EB welding process is autogenous and hence no additional materials are introduced through a filler metal, the temperature changes during welding can cause compositional changes close to the weld such as the dissolution of second phase particles. Any change in lattice parameter due to compositional changes appears to be less than the scatter inherent to this measurement process. From the scatter in the $2\theta_0$ measurements across the EB weld, the error in strain from uncertainty in the reference measurements was determined to be ± 200 $\mu\varepsilon$ as is observed in Figure 8(b). From this the error in stress was determined to be ± 40 MPa using Equation (2). As limited variability of $2\theta_0$ was observed across the weld, measurements were made at the corner of the EB welded specimens in regions that were far from the weld and which were close to free surfaces and therefore assumed to be stress free. A reference stress error of ± 40 MPa was conservatively assumed for all measurements to account for the scatter in $2\theta_0$ across the EB weld.

The residual stress components measured for each of the EB welded specimens after welding, after manufacture into C(T) blanks and after manufacture into C(T) specimens are shown in Figure 10, Figure 11 and Figure 12, respectively. The measurement lines for each configuration are indicated by dashed lines in Figure 4. The error bars shown are the maximum of the error in fitting Gaussian peaks to the measured neutron scattering angles and the error in $2\theta_0$, determined in the previous sub-section (± 40 MPa). The error in fitting Gaussian distributions to the measurement data made

using SALSA, Stress-Spec and E3 were approximately ± 20 MPa, ± 20 MPa and ± 30 - 40 MPa respectively. E3 had relatively larger peak fitting errors in comparison to the other instruments as E3 is situated at a medium flux neutron source and one requires longer counting times for these comparatively thick samples. Due to this a time compromise was made. However the peak fitting errors were approximately the same size as the strain errors due to uncertainty in $2\theta_0$.

The longitudinal component, σ_{yy}, was normal to the notch plane in the C(T) specimen and was of key interest as it would cause crack growth in subsequent CCG testing. Tensile residual stresses in the longitudinal (y) direction of between 470 MPa to 850 MPa were measured in the as-welded specimens, near the EB weld. These stresses were far greater than the base material's yield stress, σ_y, of 260 MPa, as observed in Figure 2. Such large stress components existed as the stresses were highly triaxial, where stresses in the normal (z) and transverse (x) directions were up to 550 MPa. The stress magnitudes were consistent with the peak stress of 640 MPa measured by Traore et al. (2013) in an EB welded austenitic stainless steel specimen. The length scale of the tensile stresses measured were typically 10 mm. In regions far from the EB weld, the magnitude of residual stresses reduced and became compressive. The largest compressive residual stresses, of – 270 MPa, were measured in EBW1.

Near the sides of the specimens, the transverse residual stresses, σ_{xx}, which were in the direction normal to the side faces reduced towards zero for all specimens. This is expected as far field scattering angles were used for reference, $2\theta_0$, measurements.

After the sacrificial blocks were removed in EB1, EBW4 and EBW5 the residual stresses redistributed. The redistributed stresses in the C(T) blank configuration are shown in Figure 11. Comparisons of stress components at different stages of fabrication for specimens EBW3, EBW4 and EBW5 are shown in Figure 13, Figure 14 and Figure 15 respectively. Near the EB weld region little stress redistribution was observed in EBW4 and EBW5 after removing the sacrificial blocks, as the stress components closely match those of the as-welded sample. However components σ_{xx} and σ_{yy} in EBW4 reduced by up to 200 MPa in the region 5 - 20 mm from the weld line

after machining into a C(T) blank, as shown in Figure 14. In EBW5, σ_{yy} reduced by approximately 100 MPa in this region, as shown in Figure 15.

Notches were machined into C(T) blanks using wire EDM to manufacture C(T) specimens. Figure 12 shows the magnitudes of all stress components in C(T) specimens EB2, EBW3 and EBW5. The tensile stresses measured near the EDM notches were up to 490 MPa. A comparison of stress components in the C(T) specimen with those at previous fabrication stages are shown in Figure 13 and Figure 15 for EBW3 and EBW5 respectively. The longitudinal stress component near the notch tip in EBW3 reduced by 250 MPa. However in specimen EBW5 the magnitude of stress components near the crack tip remained large, as shown in Figure 15. Stresses at quarter thickness were measured for the C(T) specimen EBW5 along line EE to assess the through thickness variation of residual stresses, and these are also shown in Figure 12. The peak longitudinal stress, σ_{yy}, at quarter thickness was measured to be 330 MPa. The reduction in magnitude of the stress components at quarter thickness indicates a through thickness variation of residual stresses.

4.2 Slitting

The strains measured during sectioning of the EBW4 C(T) blank by the three strain gauges as a function of the cut length, a, are shown in Figure 16. Data is shown for the first 50 mm of the cut only as the encapsulant surrounding the strain gauges detached from the specimen and the gauges were no longer sealed. The mean of the three strain gauges for each cut distance was used for the calculations. Noise in the measurements was removed by fitting a second order polynomial to five successive data points. These expressions were differentiated to determine $d\varepsilon/da$ at each incremental cut position.

The stress intensity factor, K, was determined using Equation (3) and is shown in Figure 17 as a function of a. The material properties: E = 205 MPa and ν = 0.29, were used and plane strain conditions were assumed in the calculation. The peak value of K is 20.7 MPa√m and was observed at 5 mm beyond the EB weld centre line. Negative values of K were obtained up until the weld which was located at a = 30 mm, showing the residual stresses imposed a compressive load on the cut tip.

The residual stress distribution in the direction normal to the cut face was calculated using Equation (4) and is shown in Figure 18. This stress component corresponds to the longitudinal (y) direction to the weld and is an average through the thickness of the specimen. Tensile stresses were measured near the weld with the peak stress at a cut distance of 30.6 mm which is in good agreement with the weld location.

4.3 The Contour Method

The averaged displacements of both cut surfaces of EBW4 following sectioning were measured using a CMM and these are shown in Figure 19. These displacements were used to determine the residual stresses in the EBW4 C(T) blank using an elastic FE analysis.

The knot spacing used to fit splines to the displacement data was determined using the procedure presented by Prime et al. (2004), where the uncertainty in stress was determined for various knot densities. Figure 20 shows knot spacings of 3 mm and greater have the smallest error, whereas the data is under smoothed for spacings of 1 mm and 2 mm as the uncertainties in stresses are large. A comparison of the stresses at mid-thickness, along line CC in Figure 4, for knot spacings of 3 mm and 4 mm is shown in Figure 21, where the peak tensile stresses are 460 MPa and 440 MPa respectively. The peak tensile stresses may have been over smoothed by a spacing of 4 mm, hence a knot spacing of 3 mm was selected in this study.

To confirm whether the FE mesh was suitably fine, the analysis was completed using two mesh densities. Figure 21 shows the longitudinal stresses along line CC for meshes with element sizes of 0.50 × 0.50 × 0.15 mm^3 and 1.00 × 1.00 × 0.15 mm^3 were identical. Both of these analyses were performed using quadratic hexahedral elements (type C3D20R).

The initial contour map of the longitudinal stress component, σ_{yy}, across the cut plane is shown in Figure 22(a). The stresses at mid-thickness, along line CC, are shown in Figure 23. The peak tensile stress had a magnitude of 460 MPa.

The error in stress due to plasticity induced during cutting may be estimated using the approach presented by Prime (2010). Using the maximum stress intensity factor

determined from slitting (K = 20.7 MPa√m) and the yield strength of the parent material as 260 MPa, the error was determined as 2%. As the peak stress is 460 MPa, the error is up to 9 MPa. This is consistent with the plasticity induced error of 2% reported by Traore et al. (2013).

The analysis was updated to correct for the "bulge error" using the procedure developed by Prime and Kastengren (2011). The initial estimate of the residual stresses were transferred to a full 3D FE model of the C(T) blank where the cutting process was simulated by incrementally removing elements, as shown in Figure 24. From this simulation the displacements associated with cut tip opening or closure were determined to apply a correction to the experimentally measured deformations. The FE mesh used to determine the contour method residual stresses was mirrored about the cut plane to create a model with 216,000 elements (type C3D20R) and 900,773 nodes. The size of the elements removed during the analysis were 0.50 × 0.50 × 0.15 mm^3. Two lines of elements were removed per cut increment which modelled an EDM cut width of 0.30 mm which was progressed in 0.50 mm steps.

In the cutting simulation the displacements, u_y, on two edges of the specimen were fixed to simulate the non-symmetric clamping arrangement shown in Figure 7. The deformation of the cut tip where the elements were removed to simulate a cut length of 8.0 mm is shown in Figure 24. The cut width was determined from the distance between two nodes at the cut tip as highlighted. As the elements were removed the stresses normal the cut surfaces were relieved. Figure 24 shows the stresses at the cut face are close to 0 MPa except at the regions very close to the crack tip which were caused by extrapolation errors in the FE analysis. The compressive stresses caused cut tip closure and the mouth had a width of 0.298 mm, as indicated. The initial distance between these nodes was 0.300 mm which was the assumed cut width of the wire EDM. Therefore the FE study predicts an additional 0.002 mm of material was removed from the specimen at this cut length. This distance must be subtracted from the CMM measured displacement data. In the FE simulation the width of the cut tip was evaluated at each incremental cut length, using a python script file. The estimated cut tip displacement (the bulge error) across the cut surface from the first iteration is shown in Figure 25. The displacements measured by CMM were up to ± 0.02 mm, as shown

in Figure 19. The bulge displacement error was found to be up to 10% of the surface displacements. The FE analysis to determine the residual stresses was repeated using the corrected displacements. The simulations to determine the cut tip displacements and residual stresses were repeated until the stress solution converged. Figure 23 shows the second and third iterations of the stress predictions along line CC, showing the solution converged after the third iteration.

The stresses across the cut surface of the EBW4 C(T) blank, where the bulge error has been accounted for, are shown in Figure 22(b). The peak tensile residual stress was determined to be 510 MPa which was 50 MPa greater than the initial estimate, shown in Figure 22(a). The inclusion of cut tip displacements also caused the centre of the tensile stress region to move towards the centreline of the C(T) blank, which was the expected weld position. The magnitudes of the weld residual stresses were greatest across the mid-thickness of the specimen, due to high constraint in these regions. The residual stresses reduced to ± 200 MPa towards the top and bottom surfaces of the specimen.

5 Discussion

The measurements made on the EB welded specimens show large residual stresses are generated by this welding process. Residual stress measurements were performed using three different methods in specimen EBW4 in the C(T) blank configuration. Comparisons of the stresses predicted by these methods are presented in Figure 26. A comparison between the longitudinal stress component, σ_{yy}, measured using ND and the contour method is shown in Figure 26(a), where the results are shown at mid-thickness of the specimen, along line CC. Slitting determines stresses that are averages through the thickness of the specimen, therefore in Figure 26(b) the stresses predicted by the contour method are also presented as through thickness averages for comparison.

The stress distributions show good agreement between the measurement methods. Peak tensile stresses were observed near the centre of the specimen width for all stress profiles which corresponded to the location of the EB weld. All the methods measured compressive stress of up to – 200 MPa in the parent material. However the

magnitudes of the peak tensile longitudinal stresses differed between the three measurement techniques. The peak tensile stress was measured as 650 MPa using ND and 510 MPa using the contour method.

Errors in the ND measurements near the weld may have existed due to the use of a reference scattering angle, $2\theta_o$ determined from the parent material. A systematic variation in $2\theta_o$ was not identified when measuring reference coupons (Figure 8(b) and Figure 9) and from these measurements an error of up to ± 40 MPa was determined from the scatter in reference strain measurements. This is shown by the error bars in the ND measurements presented.

The peak tensile stress measured by slitting in EBW4 was 450 MPa. This is greater than the corresponding stress measured using the contour method where the thickness averaged peak tensile stress was 350 MPa, as shown in Figure 22(b). One possible contribution to this difference in the results could be the use of non-ideal clamping strategy for the contour method. During sectioning of the EBW4 C(T) blank, the sample was only clamped on one side of the cut plane to permit slitting measurements to be made. Ideally for the contour method the specimen should be rigidly clamped either side of the cut. Further investigation is required to explore the differences obtained between the contour method and slitting measurements. Full 3D modelling of the cutting process is proposed for future work to study the mechanism of deformation, the possibility of plasticity at the cut tip during cutting and the effect of non-ideal clamping arrangement (Hosseinzadeh et al., 2016; Muránsky et al., 2016).

The stress distributions measured at each of the C(T) specimen fabrication stages are generally consistent, as the stress components are within ± 100 MPa for large regions of many of the specimens and within the scatter inherent in the ND technique. This shows repeatability in the ND measurement technique. Samples EBW4 and EBW5 were tested using different instruments at various fabrication stages. The changes in stresses observed in Figure 14 and Figure 15 appear to be due to stress redistribution and therefore the different ND instruments used in this study have produced consistent measurements. Two systematic differences were observed between the test specimens: specimen EBW1 had markedly larger compressive longitudinal stresses, σ_{yy}, in regions far from the weld, and the stress magnitudes in specimens EB1, EB2

and EBW5 were larger than those observed in EBW3 and EBW4. The cause of these differences are discussed below.

The compressive stress in the longitudinal direction, σ_{yy}, in EBW1 were up to 200 MPa greater than those measured in EBW3, EBW4 and EBW5 in the as-welded configuration, as shown in Figure 10(a). In specimen EBW1 a wide fusion zone was observed which was caused by the increased heat input during the EB welding process. Due to this, the tensile stresses near the weld occurred over longer length scales in comparison to samples EBW3, EBW4 and EBW5. The integrated longitudinal stress component across the transverse – normal (x–z) plane must equal zero to satisfy equilibrium. Therefore larger compressive stresses existed in EBW1 to balance the tensile region near the weld. Once the sacrificial material in EBW3, EBW4 and EBW5 were removed, the magnitude of the compressive residual stresses increased, as shown in Figure 14 and Figure 15. Specimens EBW3, EBW4 and EBW5 had material beneath the EB weld to contain the weld root. This material provided additional constraint to the specimen and is likely to have contained compressive stresses to balance the tensile stresses induced in the EB weld region. Once the sacrificial material was removed in EBW4 and EBW5, the compressive σ_{yy} component reduced to approximately – 200 MPa to balance the near weld tensile stresses.

The magnitude of residual stresses in specimens EB1, EB2 and EBW5 appear greater than those in EBW3 and EBW4, as shown by Figure 10, Figure 11 and Figure 12. Specimen EB1 and EB2 contained a MMA weld. The measurement line in EB1 and EB2 was within the MMA weld's HAZ and therefore the material in this region had been cyclically hardened during welding. Specimen EBW5 was made from pre-compressed material where work hardening increased the material's tensile strength in comparison to material in the as-received condition, as shown in Figure 2. Therefore the large residual stresses that were observed in samples EB1, EB2 and EBW5 existed due to the work hardened state of the materials.

Measurements were made, using the ND technique, at various stages of manufacturing the EB welded C(T) specimens to enable the redistribution of the residual stresses to be determined. The largest change in residual stress occurred following insertion of the EDM notches in the C(T) specimens. The notches extended

beyond the EB weld region which partially removed this misfit between the EB weld and the surrounding material, and hence caused a reduction in residual stresses.

Davies et al. (2010) measured residual stresses in Type 316 stainless steel MMA weldments, which did not contain EB welds, which had residual stresses of ± 100 MPa. Following extension of the EDM notch in EB2 EDM2 to a/W = 0.57, the residual stress components redistributed to a magnitude less than ± 100 MPa, and the effect of the EB weld appears to be small. To conduct CCG testing in C(T) specimens where EB welding is used to conserve ex-service material, the influence of residual stresses must be small. To ensure this, the pre-crack or notch must be sufficiently far from the EB weld. The specimens tested in this study show the notch must extend 9 mm beyond the centre of the EB weld.

The longitudinal stress component, σ_{yy}, was large ahead of the EDM notch in specimens EBW5 (a/W = 0.44) and EB2 EDM1 (a/W = 0.50). These specimens were made using hardened material and therefore the stresses were greater than those observed in EBW3. These large stresses would enhance crack growth in subsequent CCG tests. Therefore EB welded C(T) specimens with pre-cracks or notches extending short distances beyond the EB weld are ideal for conducting CCG testing under the influence of residual stresses. The measurements presented in this study show that the residual stress fields induced by EB welding are repeatable, thereby allowing a large number of fracture mechanics specimens to be made with consistent crack tip stress fields.

6 Conclusions

C(T) specimens were fabricated using EB welds to assess the influence of residual stresses on CCG and to attach extension pieces onto weldments in order to conserve ex-service material. Residual stress measurements showed that large tensile stresses, of up to three times the base material's room temperature yield stress, were induced by EB welding. Stress redistribution occurred during fabrication into C(T) specimens. However the stresses remained large where the EDM notch extended up to 5 mm beyond the EB weld, as stresses of up to twice the base material's yield stress were measured in the C(T) specimens ahead of the notch tip. These high stresses would

increase the crack driving force in subsequent CCG tests. Therefore this welding process must be used with caution when adopted for the purpose of conserving ex-service material in fracture mechanics specimens. Extending the notch to 9 mm beyond the EB weld allowed the crack tip stresses to redistribute and reduce to small magnitudes.

Residual stress measurements were made using ND, slitting and the contour method, which were generally in close agreement with each other. However residual stresses measured by the contour method were up to 150 MPa less than those predicted by ND and slitting, in a small region near the EB weld. Possible sources of error were identified in the ND and the contour method techniques. The stress error from the change in reference scattering angle across the weld, caused by microstructural or compositional variations, was quantified as ± 40 MPa. Sectioning of the EB weld sample for the contour method using wire EDM was performed using asymmetric clamping to permit back face strains to be measured for slitting. This non-ideal clamping arrangement may have caused errors in the measurement. The errors associated with cut tip displacement were estimated by simulation of the cutting process using a FE analysis. By including these displacements in the contour method analysis the agreement of the stress predictions between that measured by ND and slitting improved.

A comparison of EB weld residual stresses measured in various test samples showed the magnitude of residual stresses was dependent on the material's yield strength. Material that had been work hardened, due to pre-compression or cyclically hardened by a nearby multi-pass weld, had larger residual stresses than those in specimens made of material in the as-received condition.

7 Acknowledgements

This research project has been supported by the European Commission under the 7th Framework Programme through "Research Infrastructures" action of the "Capacities" Programme, contract number CP-CSA_INFRA-2011-1.1.17 Number 283883 NMI3 II. The authors would like to acknowledge FRM-II, HZB and ILL for the provision of beam time to perform the ND measurements. Dr. Catrin M. Davies acknowledges the

Engineering and Physical Sciences Research Council (EPSRC), UK for the support under Grant EP/I004351/1. The authors would like to thank Pete Ledgard from the Open University for his invaluable help with the slitting and contour measurements. This paper is published by permission of EDF Energy Nuclear Generation Ltd.

8 References

ABAQUS, 2011. Version 6.11. Dassault Systèmes.

ASTM, 2013. ASTM E1457-13 Standard Test Method for Measurement of Creep Crack Growth Times in Metals, ASTM International.

Boin, M., Wimpory, R.C., Randau, C., 2014. Improving beamtime efficiency for residual stress neutron experiments. Mater. Sci. Forum 777, 7–11.

Bueckner, H.F., 1958. The propagation of cracks and the energy of elastic deformation. Trans. ASME 80, 1225–1230.

Coleman, M.C., Miller, D., Stevens, R.A., 1998. Reheat cracking and strategies to assure integrity of Type 316 welded components. In: Integrity of High Temperature Welds. Professional Engineering Publishing Limited, London, pp. 169–180.

Davies, C.M., Hughes, D., Wimpory, R.C., Dean, D.W., Nikbin, K.M., 2010. Measurements of residual stresses in 316 stainless steel weldments. In: Proceedings of the ASME 2010 Conference on Pressure Vessels and Piping, 6. Bellevue, Washington, USA, pp. 1265–1273. doi:10.1115/PVP2010-25034, Parts A and B. ASME.

EDF Energy, 2014. R5: Assessment Procedure for the High Temperature Response of Structures. Issue 3 Revision 002. Gloucester, UK.

Fett, T., Munz, D., 1997. Stress intensity factors and weight functions. Computational Mechanics Publications. The University of Michigan.

Hill, M.R., 2013. The slitting method. In: Schajer, G.S. (Ed.), Practical Residual Stress Measurement Methods. John Wiley & Sons Ltd, pp. 89–108. doi:10.1002/9781118402832.ch4.

Hofmann, M., Schneider, R., Seidl, G.A., Rebelo-Kornmeier, J., Wimpory, R.C., Garbe, U., Brokmeier, H.G., 2006. The new materials science diffractometer STRESS-SPEC at FRM-II. Phys. B Condens. Matter 385–386, 1035–1037. doi:10.1016/j.physb.2006.05.331.

Holden, T.M., 2013. Neutron diffraction. In: Schajer, G. (Ed.), Practical Residual Stress Measurement Methods. John Wiley & Sons Ltd, pp. 195–224.

Hosseinzadeh, F., Traore, Y., Bouchard, P.J., Muránsky, O., 2016. Mitigating cutting induced plasticity in the contour method, part 1: experimental. Int. J. Solids Struct. 94–95, 247–253. doi:10.1016/j.ijsolstr.2015.12.034.

Hutchings, M.T., Withers, P.J., Holden, T.M., Lorentzen, T., 2005. Introduction to the Characterization of Residual Stress by Neutron Diffraction. Taylor & Francis.

Kapadia, P., Davies, C.M., Dean, D.W., Nikbin, K.M., 2015. Creep crack growth testing under secondary and combined loading. In: Proceedings of the ASME 2015 Pressure Vessels and Piping Conference, 6A doi:10.1115/PVP2015-45222, Materials and Fabrication. p. V06AT06A042.

Mehmanparast, A., Davies, C.M., Dean, D.W., Nikbin, K., 2016. Effects of plastic

prestraining level on the creep deformation, crack initiation and growth behaviour of 316H stainless steel. Int. J. Press. Vessel Pip. 141, 1–10. doi:10.1016/j.ijpvp.2016.03.013.
Mehmanparast, A., Davies, C.M., Dean, D.W., Nikbin, K.M., 2013. The influence of pre-compression on the creep deformation and failure behaviour of Type 316H stainless steel. Eng. Fract. Mech. 110, 52–67. doi:10.1016/j.engfracmech.2013.08.006.
Muránsky, O., Hamelin, C.J., Hosseinzadeh, F., Prime, M.B., 2016. Mitigating cutting induced plasticity in the contour method. Part 2: numerical analysis. Int. J. Solids Struct. 94–95, 254–262. doi:10.1016/j.ijsolstr.2015.12.033.
Pirling, T., Bruno, G., Withers, P.J., 2006. SALSA – a new instrument for strain imaging in engineering materials and components. Mater. Sci. Eng. A 437, 139–144. doi:10.1016/j.msea.2006.04.083.
Prime, 1999. Measuring residual stress and the resulting stress intensity factor in compact tension specimens. Fatigue Fract. Eng. Mater. Struct. 22, 195–204. doi:10.1046/j.1460-2695.1999.00155.x.
Prime, M.B., 2010. Plasticity effects in incremental slitting measurement of residual stresses. Eng. Fract. Mech. 77, 1552–1566. doi:10.1016/j.engfracmech.2010.04.031.
Prime, M.B., DeWald, A.T., 2013. The contour method. In: Schajer, G.S. (Ed.), Practical Residual Stress Measurement Methods. John Wiley & Sons Ltd, pp. 109–138.
Prime, M.B., Kastengren, A.L., 2011. The contour method cutting assumption: error minimization and correction. In: Experimental and Applied Mechanics, 6. Springer, pp. 233–250.
Prime, M.B., Sebring, R.J., Edwards, J.M., Hughes, D.J., Webster, P.J., 2004. Laser surface-contouring and spline data-smoothing for residual stress measurement. Exp. Mech. 44, 176–184. doi:10.1007/BF02428177.
Schindler, H.-J., Bertschinger, P., 1997. Some steps towards automation of the crack compliance method to measure residual stress distributions. In: Proceedings of the Fifth International Conference on Residual Stress. Linköping.
Traore, Y., Paddea, S., Bouchard, P.J., Gharghouri, M.A., 2013. Measurement of the residual stress tensor in a compact tension weld specimen. Exp. Mech. 53, 605–618. doi:10.1007/s11340-012-9672-7.
Withers, P.J., Preuss, M., Steuwer, A., Pang, J.W.L., 2007. Methods for obtaining the strain-free lattice parameter when using diffraction to determine residual stress. J. Appl. Crystallogr. 40, 891–904. doi:10.1107/S0021889807030269.

Tables

Table 1 List of EB welded C(T) specimens and the instrument used for ND measurements

Specimen ID	ND after welding	ND on C(T) blank	ND on C(T) specimen
EB1	–	Stress-Spec, FRM II	–
EB2	–	–	Stress-Spec, FRM II
EBW1	E3, HZB	–	–
EBW3	SALSA, ILL	–	SALSA, ILL
EBW4	SALSA, ILL	E3, HZB	–
EBW5	SALSA, ILL	SALSA, ILL	Stress-Spec, FRM II

Figures

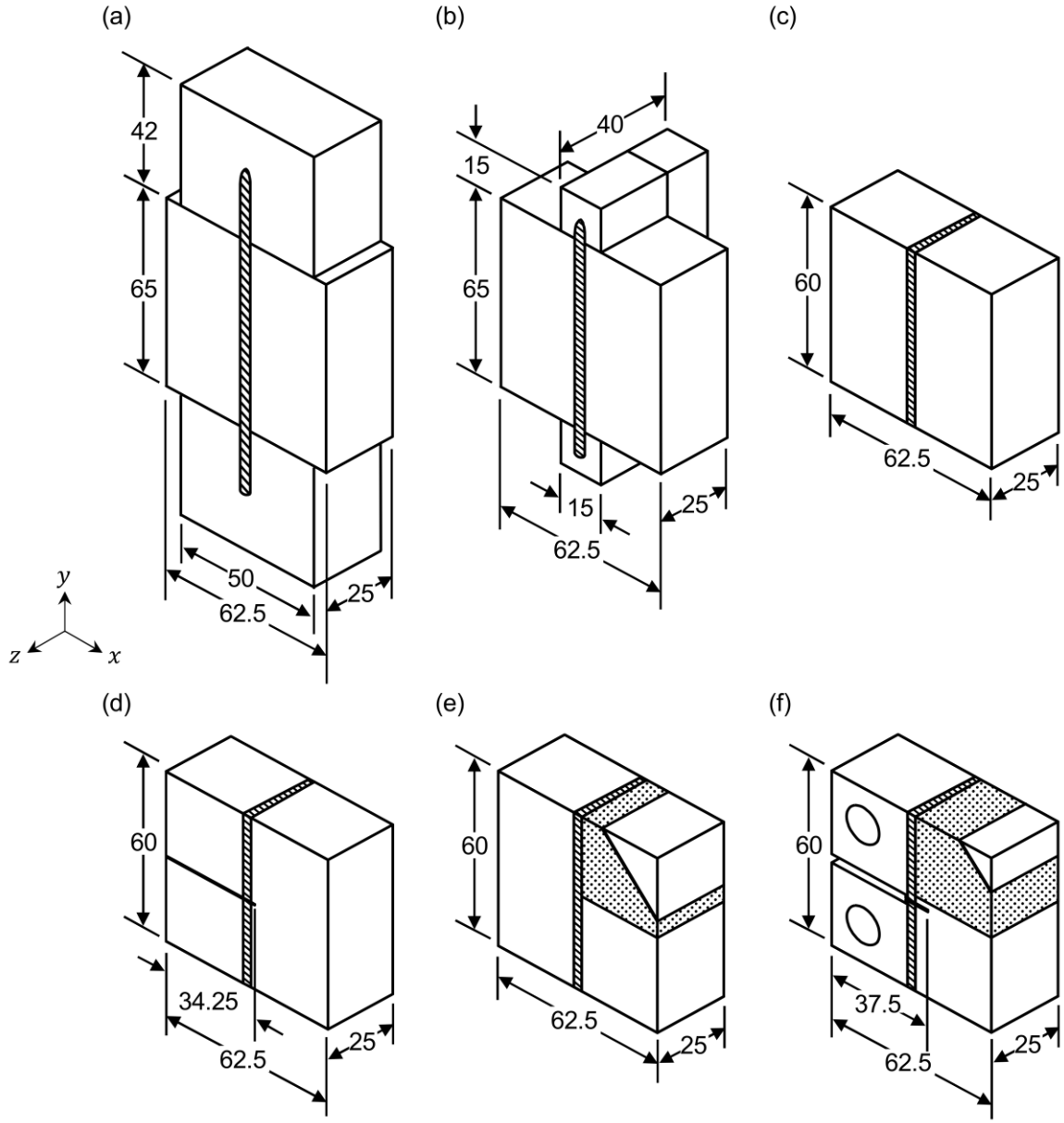

Figure 1 (a) EBW1 in the as-welded configuration, (b) EBW3, EBW4 and EBW5 in the as-welded configuration, (c) EBW3, EBW4 and EBW5 machined into a C(T) blank, (d) EBW3, EBW4 and EBW5 with an EDM notch, (e) EB1 containing a MMA weld in a C(T) blank configuration and (f) a C(T) specimen machined from EB2 containing a MMA weld. The EB and MMA welds are shown by striped and dotted patterns respectively.

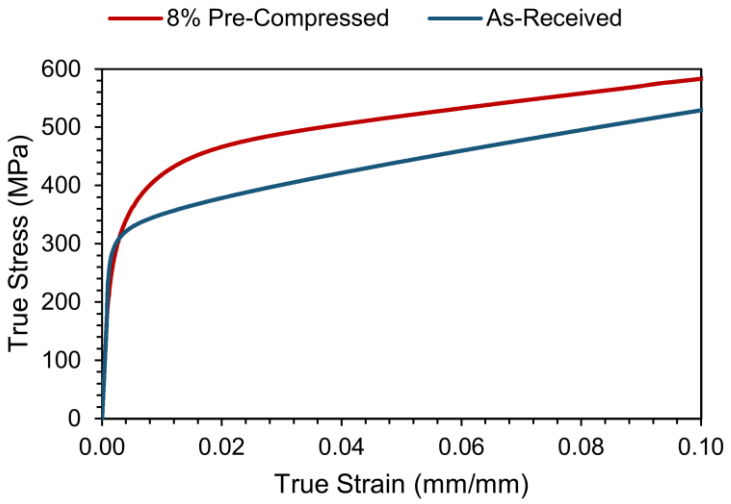

Figure 2 Tensile response of ex-service Type 316H stainless steel in the as-received and 8% pre-compressed material conditions at room temperature. Graph reproduced using data from (Mehmanparast et al., 2016).

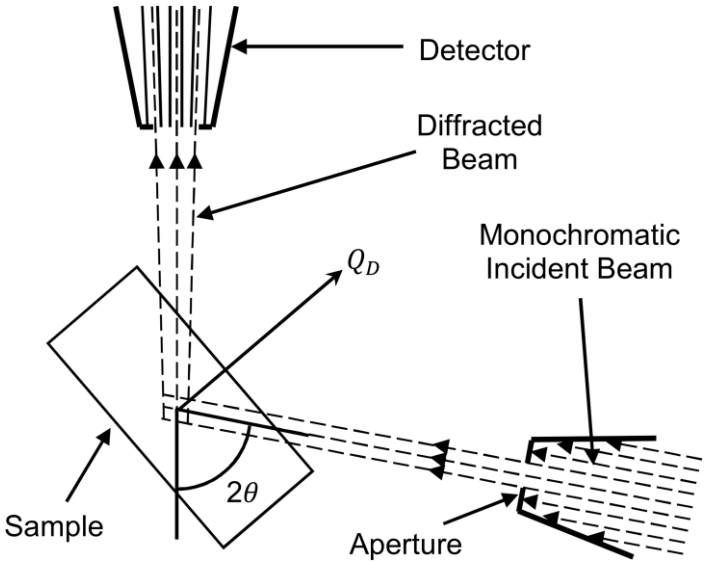

Figure 3 Measuring geometry on monochromatic stress diffractometers. Beam shaping optics can be slit apertures or radial focussing collimators, depending on the instrument used.

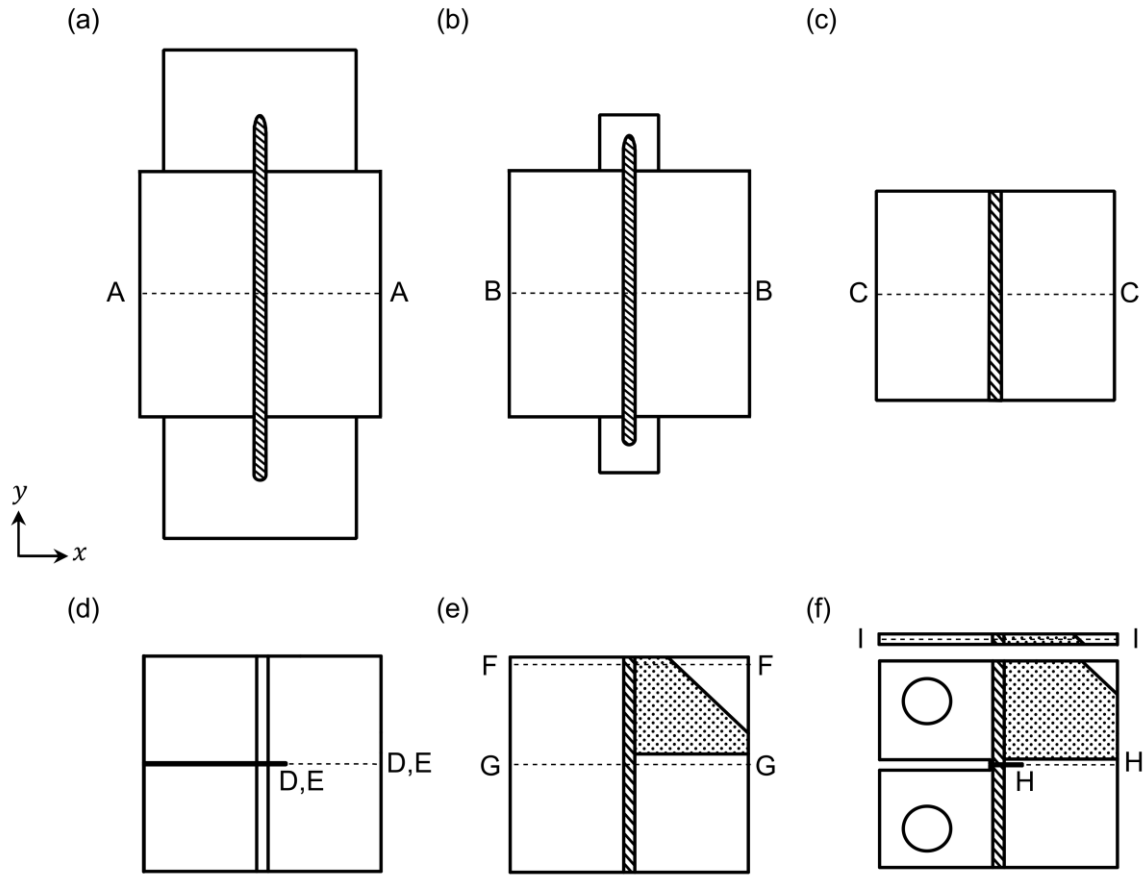

Figure 4 Dashed lines indicating measurement lines in samples (a) as-welded EBW1, (b) as-welded EBW3, EBW4 and EBW5, (c) EBW3, EBW4 and EBW5 C(T) blank, (d) EBW3 and EBW5 C(T) specimen, (e) EB1 C(T) blank, (f) EB2 C(T) specimen and EB2 reference sample, all measurement lines were at mid-thickness except line EE which was at quarter thickness. The EB and MMA welds are shown by striped and dotted patterns respectively.

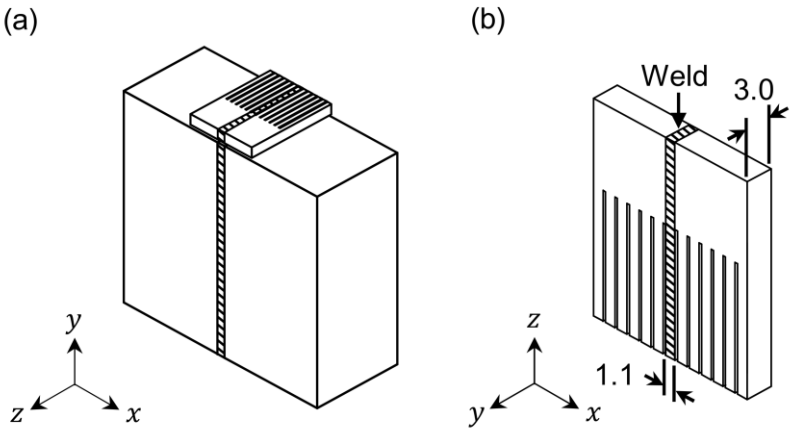

Figure 5 (a) Diagram showing the location the toothcomb specimen was machined from in specimen EBW4 and (b) the geometry of the toothcomb specimen

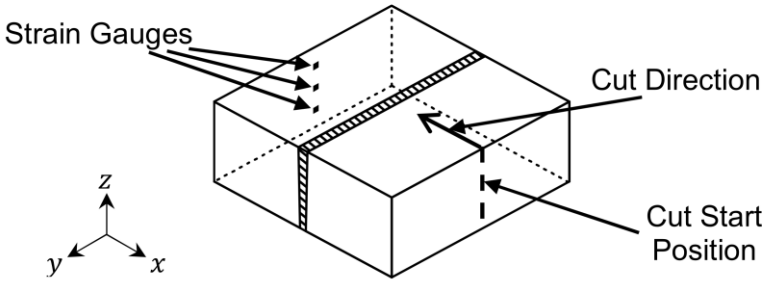

Figure 6 EBW4 C(T) blank showing strain gauge locations for slitting

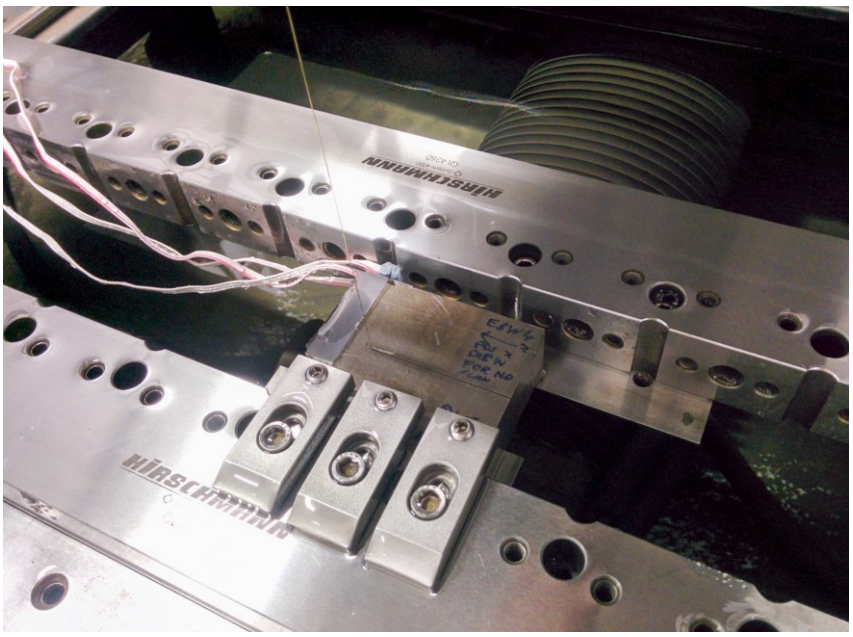

Figure 7 EBW4 C(T) blank during cutting for residual stress measurement by slitting

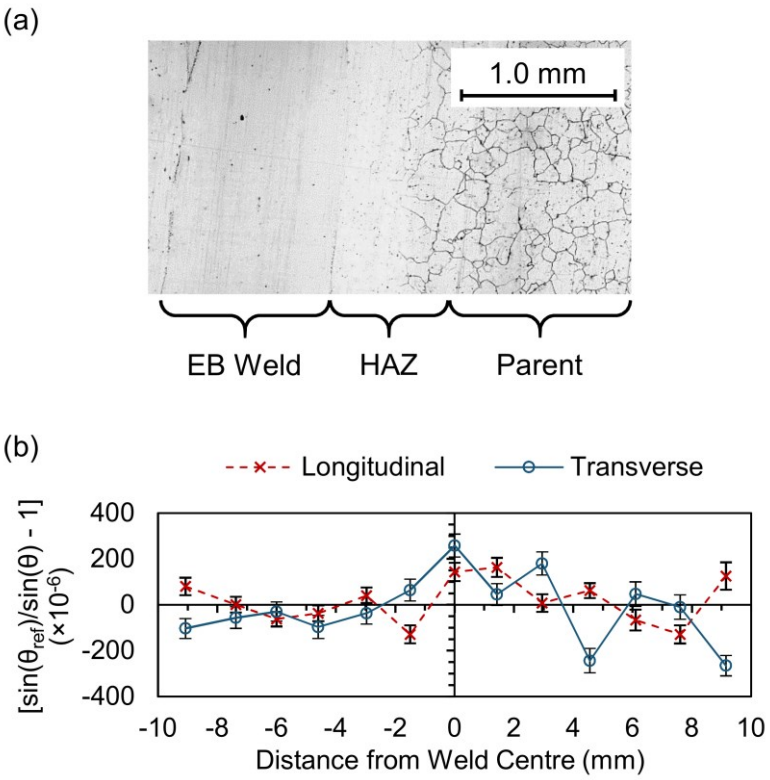

Figure 8 (a) Microstructure in EB weld region and (b) reference diffraction angles measured across the toothcomb specimen from specimen EBW4

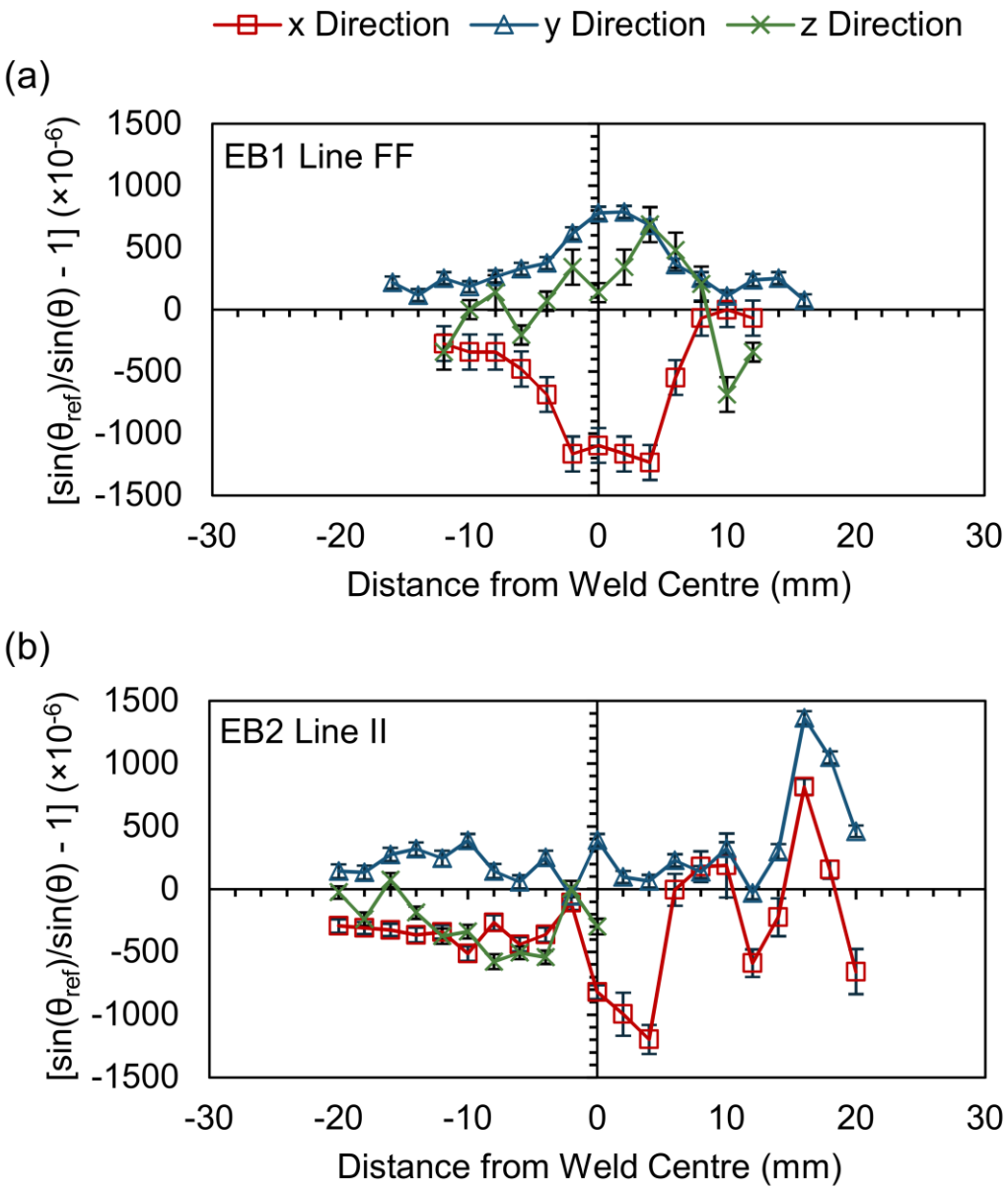

Figure 9 Reference diffraction angle measurements made in (a) EB1 and (b) EB2

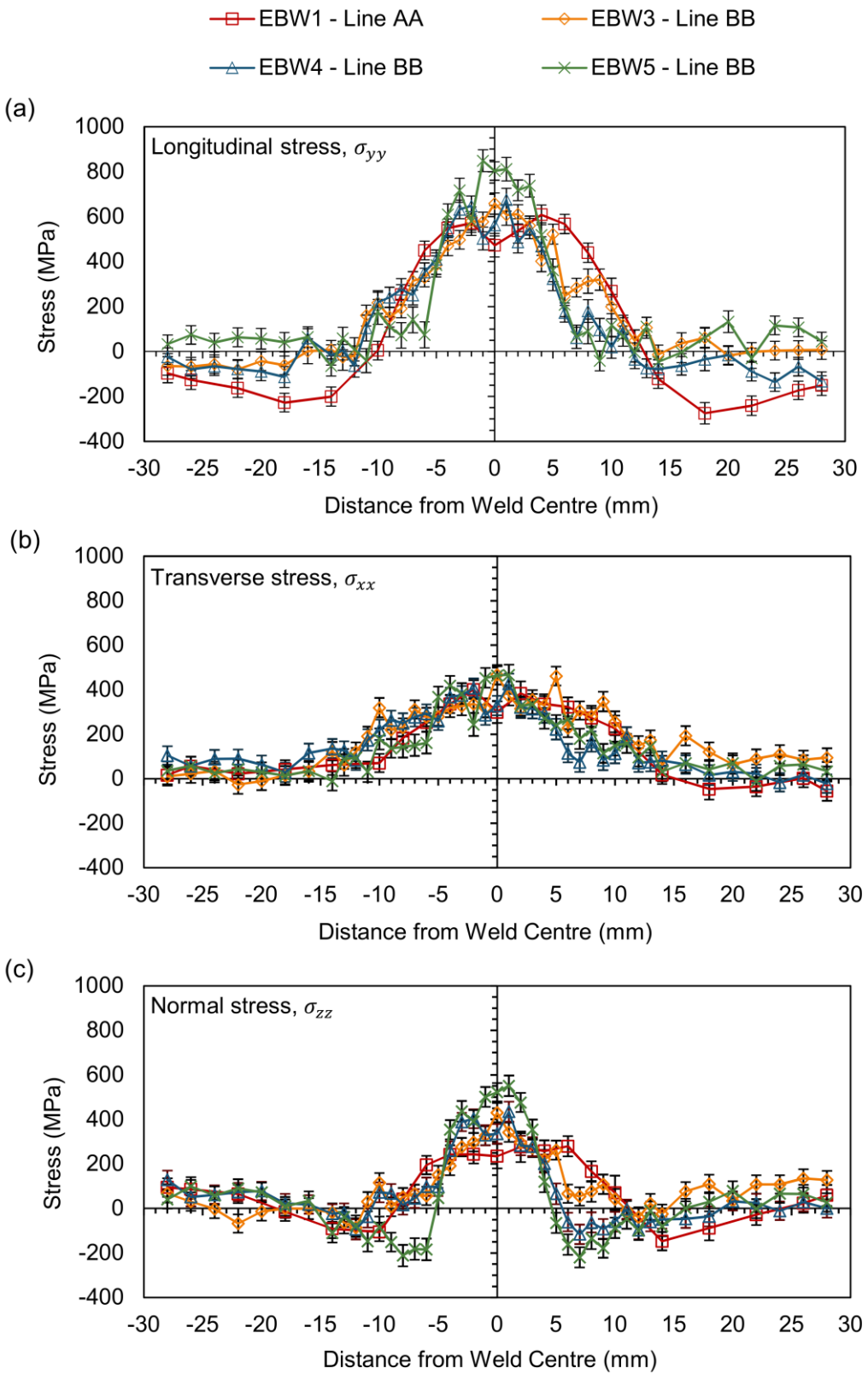

Figure 10 Residual stress components (a) σ_{yy}, (b) σ_{xx} and (c) σ_{zz} in specimens following welding

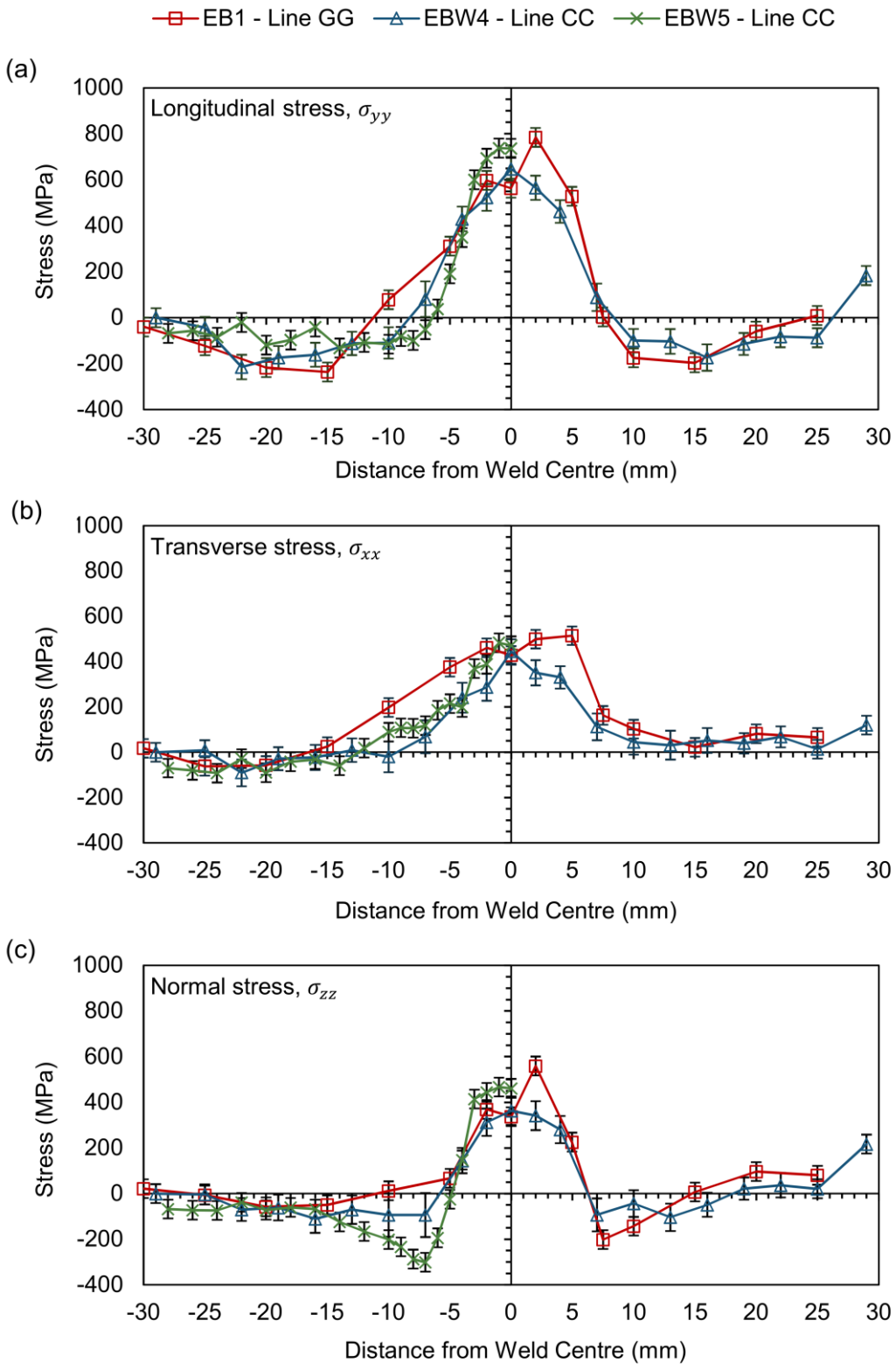

Figure 11 Residual stress components (a) σ_{yy}, (b) σ_{xx} and (c) σ_{zz} in C(T) blanks

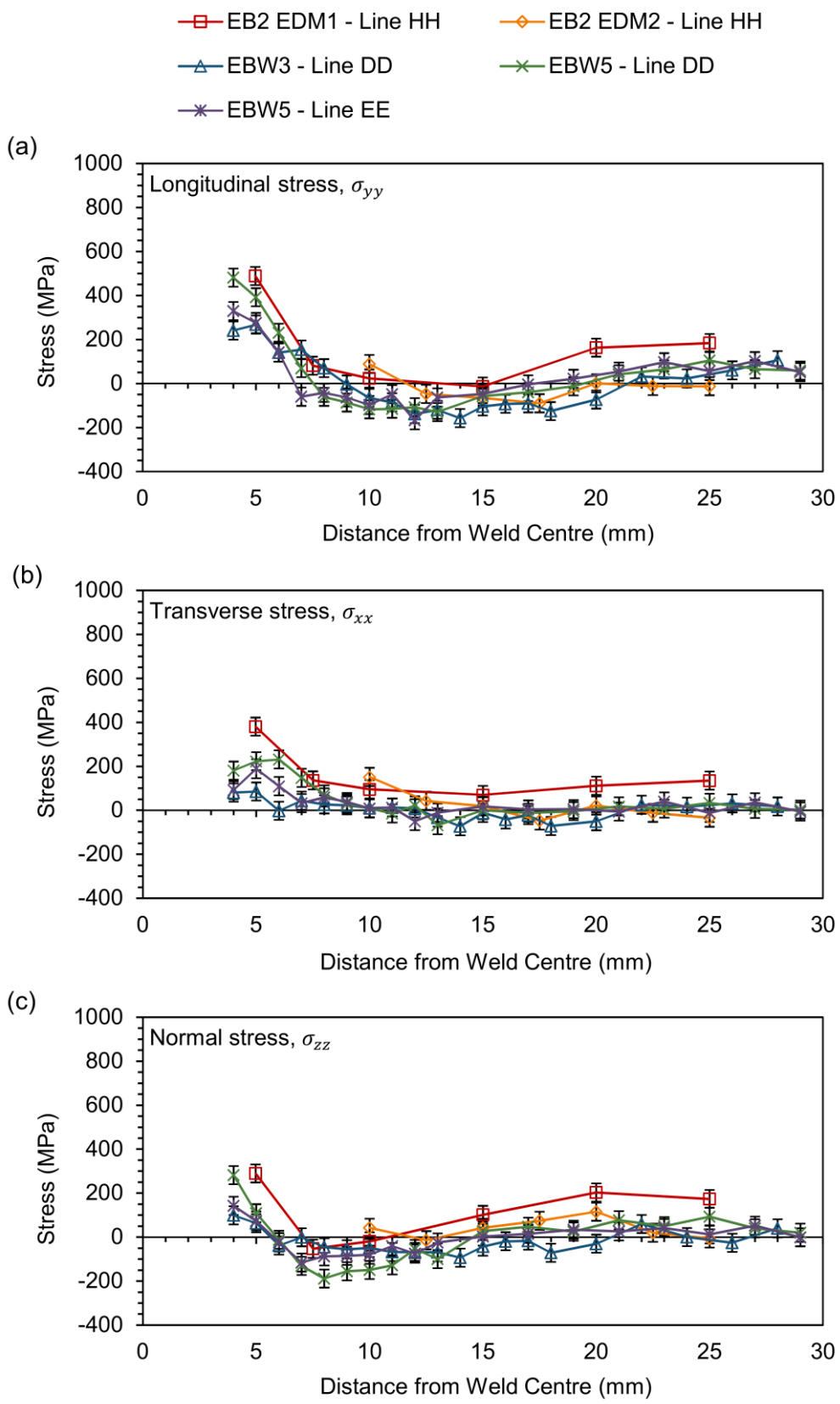

Figure 12 Residual stress components (a) σ_{yy}, (b) σ_{xx} and (c) σ_{zz} in C(T) specimens

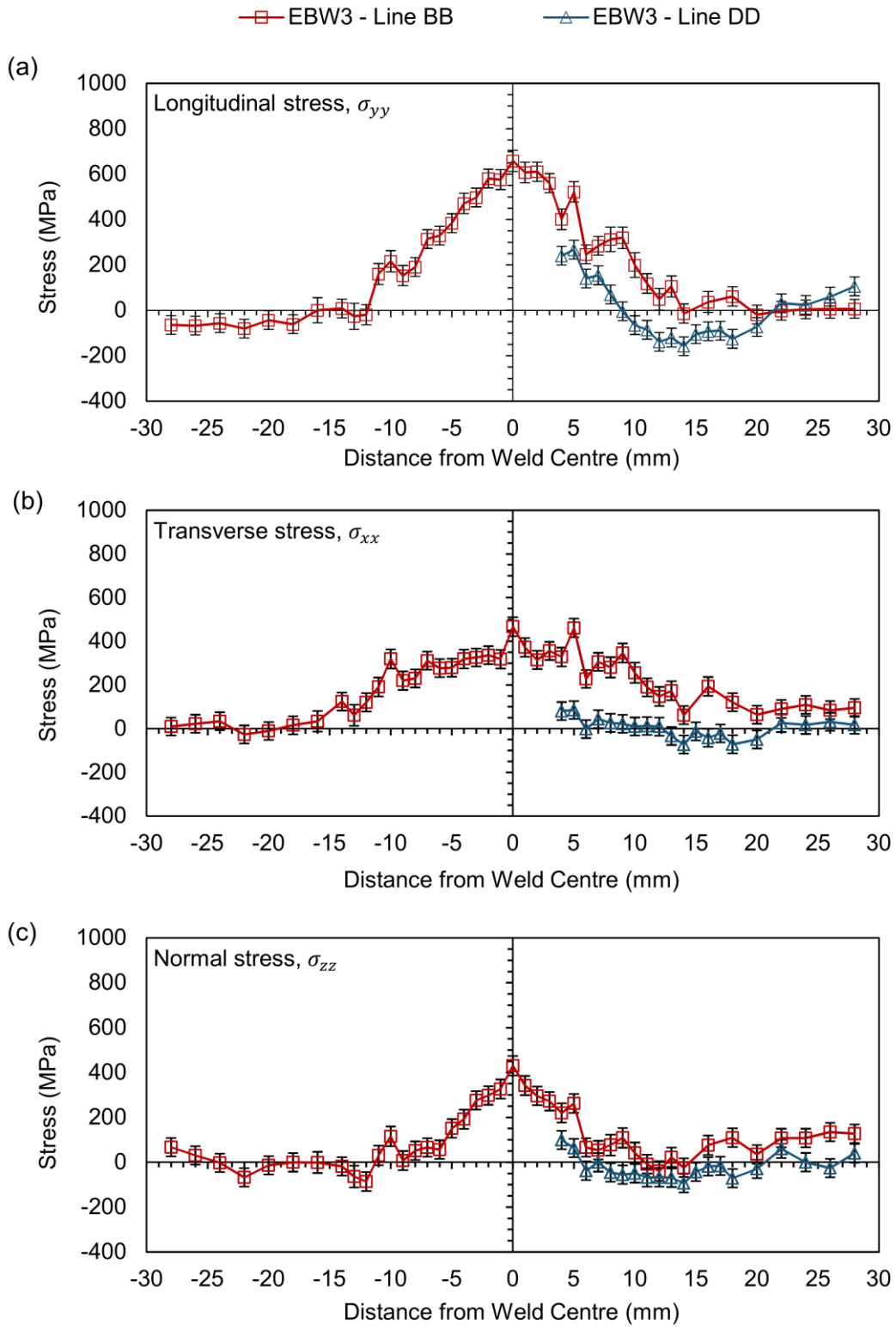

Figure 13 Redistribution of residual stress components (a) σ_{yy}, (b) σ_{xx} and (c) σ_{zz} during fabrication of specimen EBW3

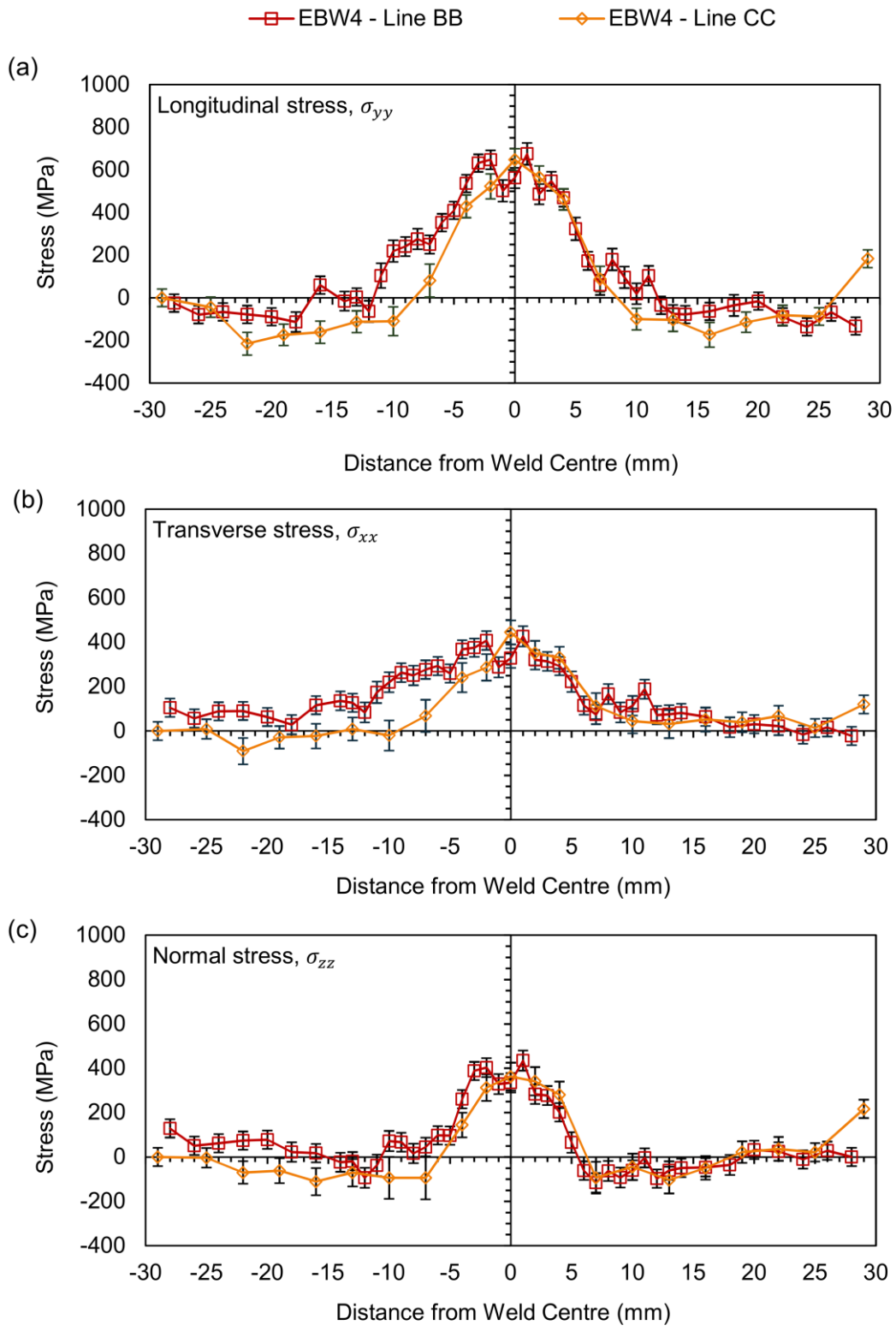

Figure 14 Redistribution of residual stress components (a) σ_{yy}, (b) σ_{xx} and (c) σ_{zz} during fabrication of specimen EBW4

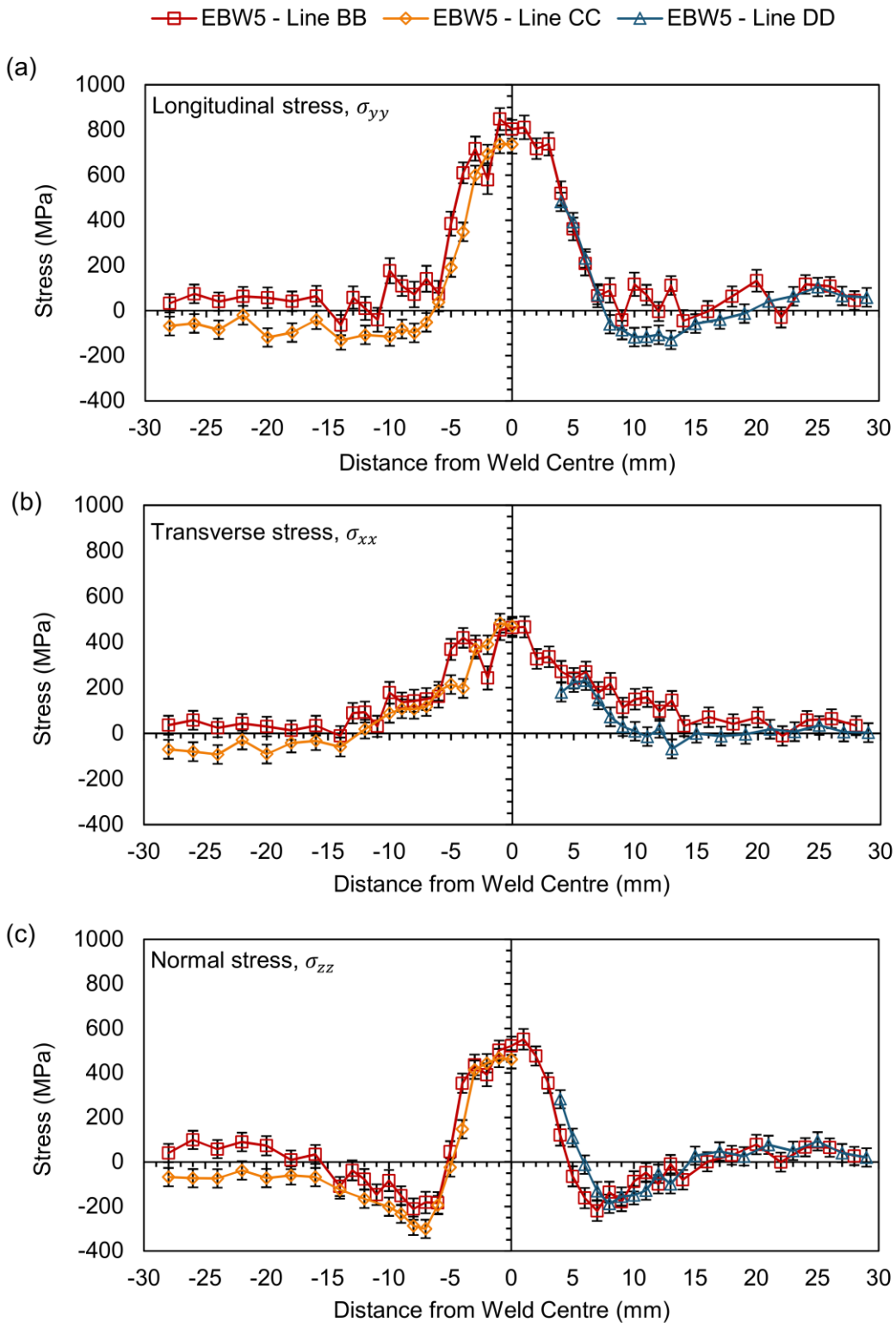

Figure 15 Redistribution of residual stress components (a) σ_{yy}, (b) σ_{xx} and (c) σ_{zz} during fabrication of specimen EBW5

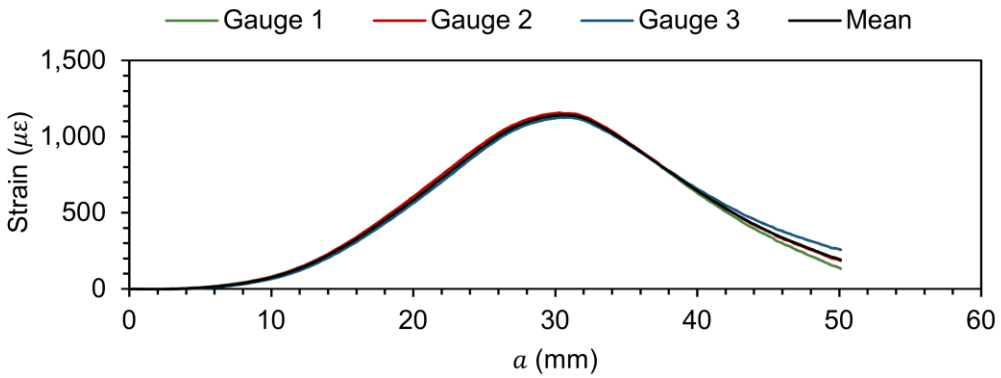

Figure 16 Relaxed strains obtained from the slitting method measurement on EBW4 C(T) blank.

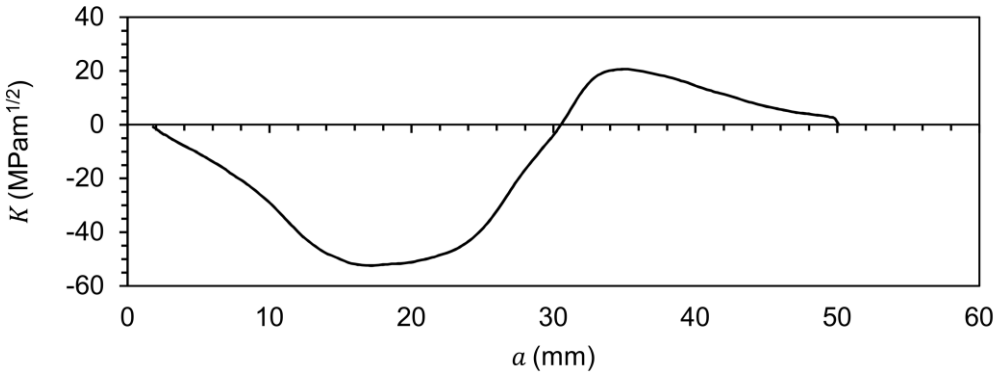

Figure 17 Stress intensity factor for EBW4 C(T) blank determined by slitting

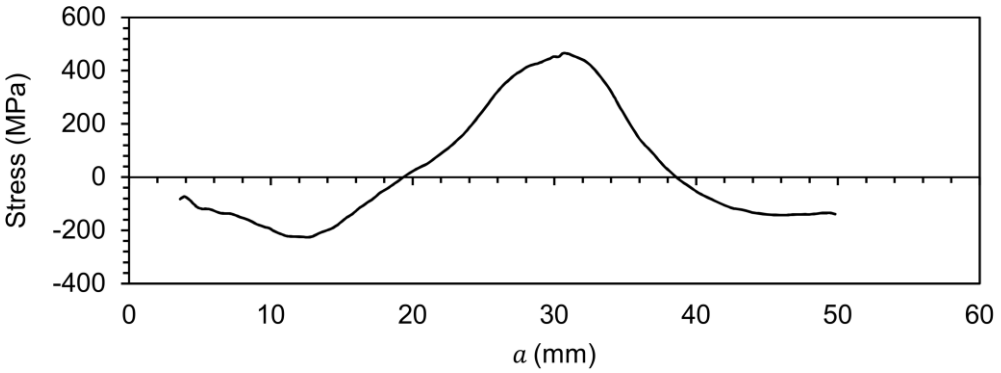

Figure 18 Longitudinal stress, σ_{yy}, for EBW4 C(T) blank determined from the slitting method

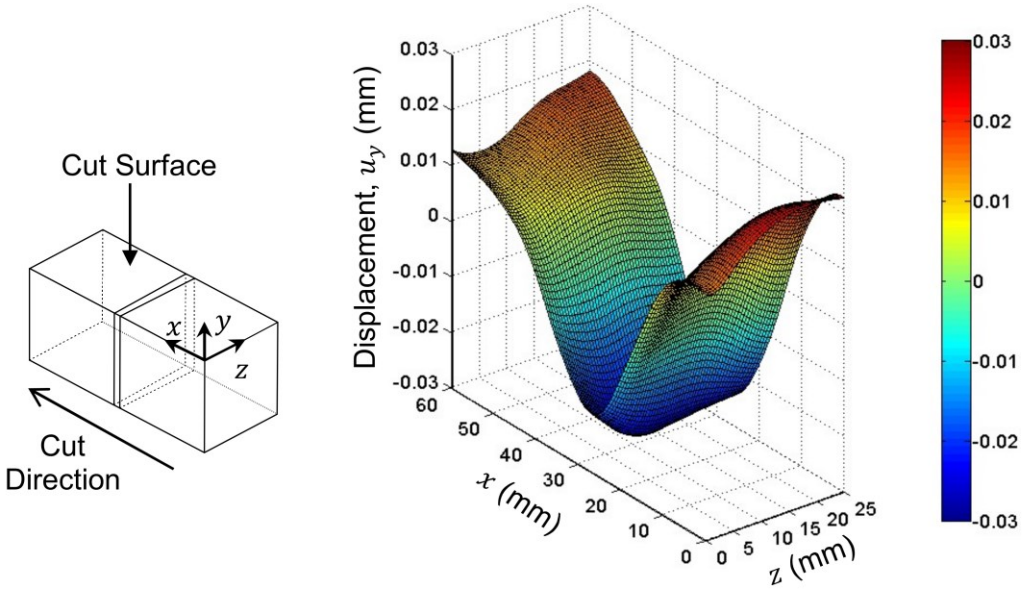

Figure 19 Averaged and smoothed displacements evaluated at nodal positions of the contour FE model for EBW4 C(T) blank, deformation units are in mm.

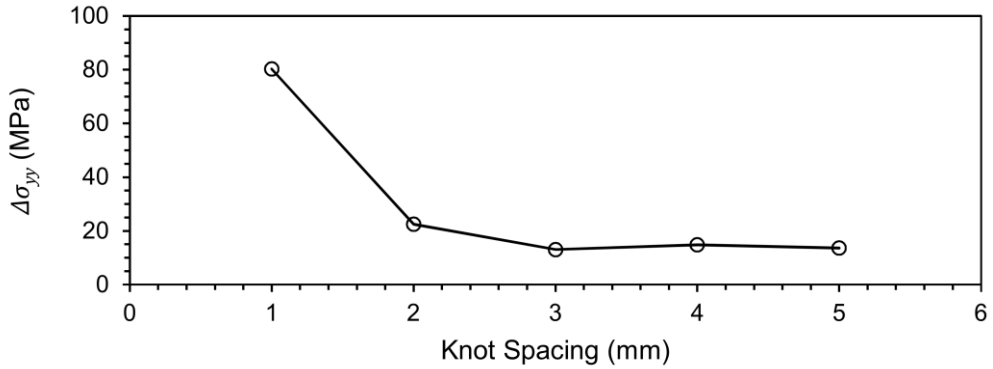

Figure 20 Uncertainty in stress from the selection of spline knot spacing to fit the contour method displacement data, following the procedure presented by Prime et al. (2004)

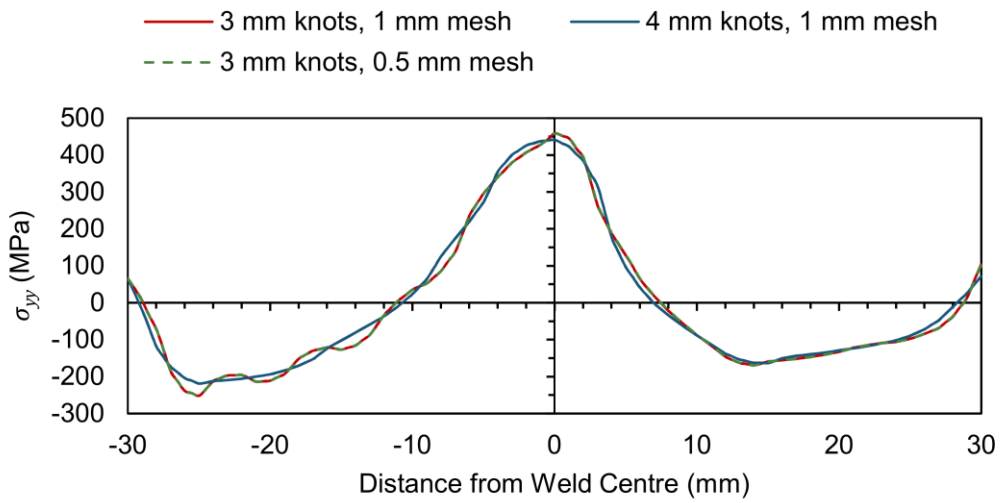

Figure 21 Sensitivity studies for the longitudinal weld residual stresses, σ_{yy}, along mid-thickness of EBW4 C(T) blank determined by the contour method, cut direction from left to right

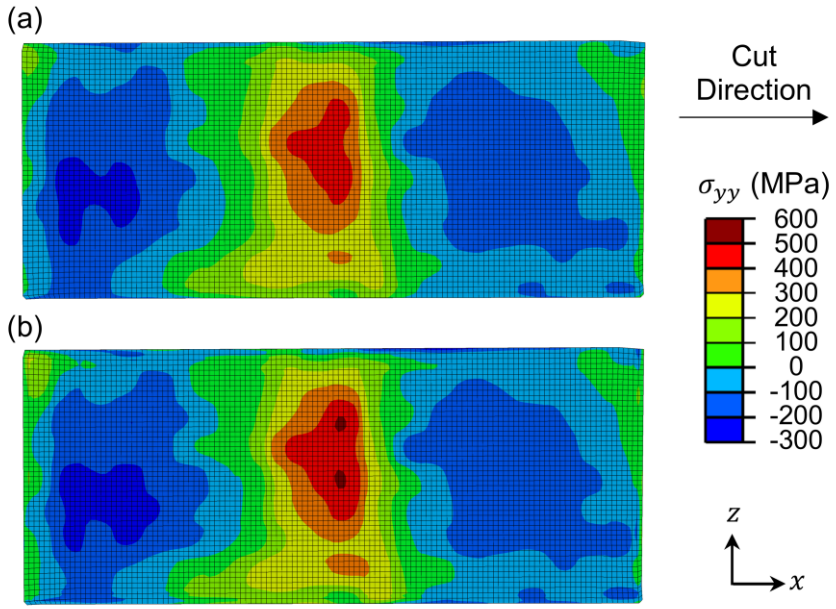

Figure 22 Longitudinal weld residual stresses, σ_{yy}, in EBW4 C(T) blank determined by the contour method (a) initial estimate (b) corrected for the bulge error

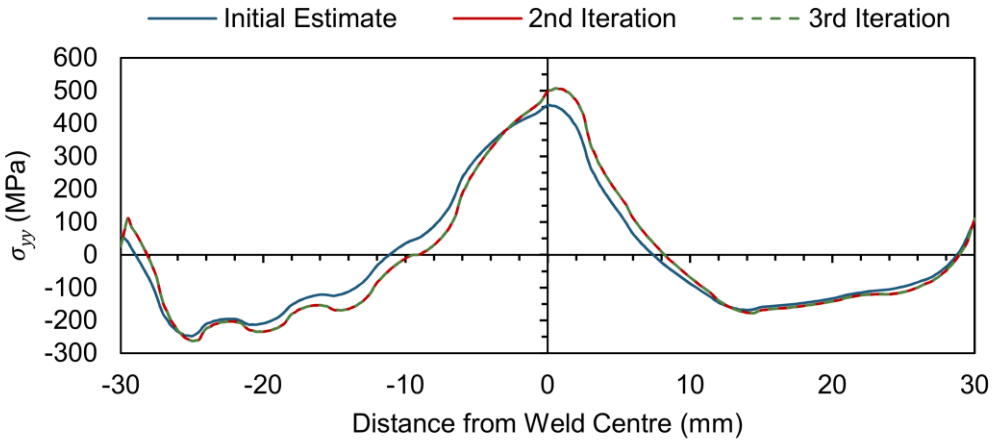

Figure 23 Longitudinal weld residual stresses, σ_{yy}, along mid-thickness of EBW4 C(T) blank determined by the contour method, cut direction from left to right

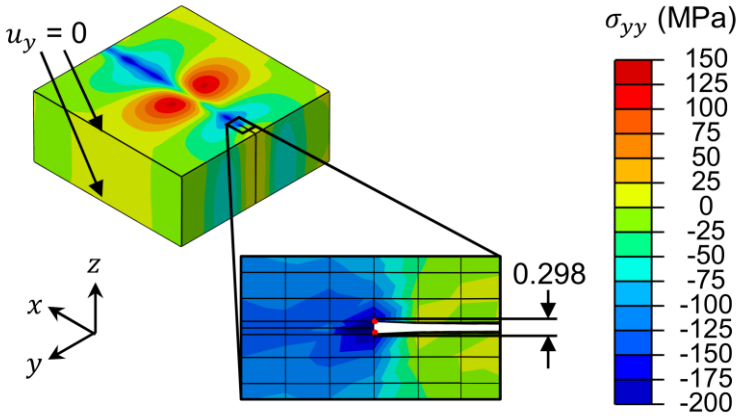

Figure 24 Simulating cutting of EBW4 C(T) blank to determine the deformation of the cut tip

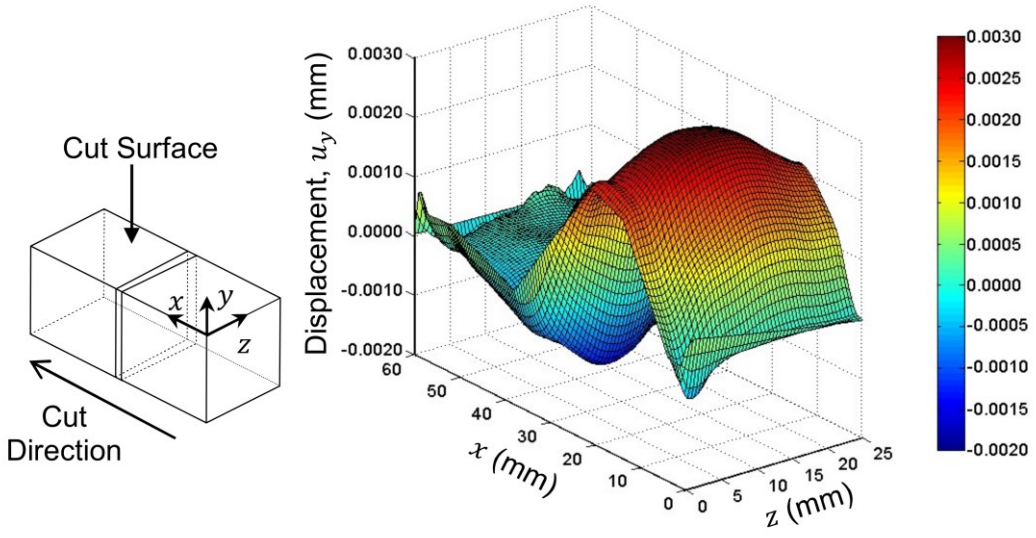

Figure 25 The cut tip deformation map (bulge error) obtained from the FE correction procedure for EBW4 C(T) blank

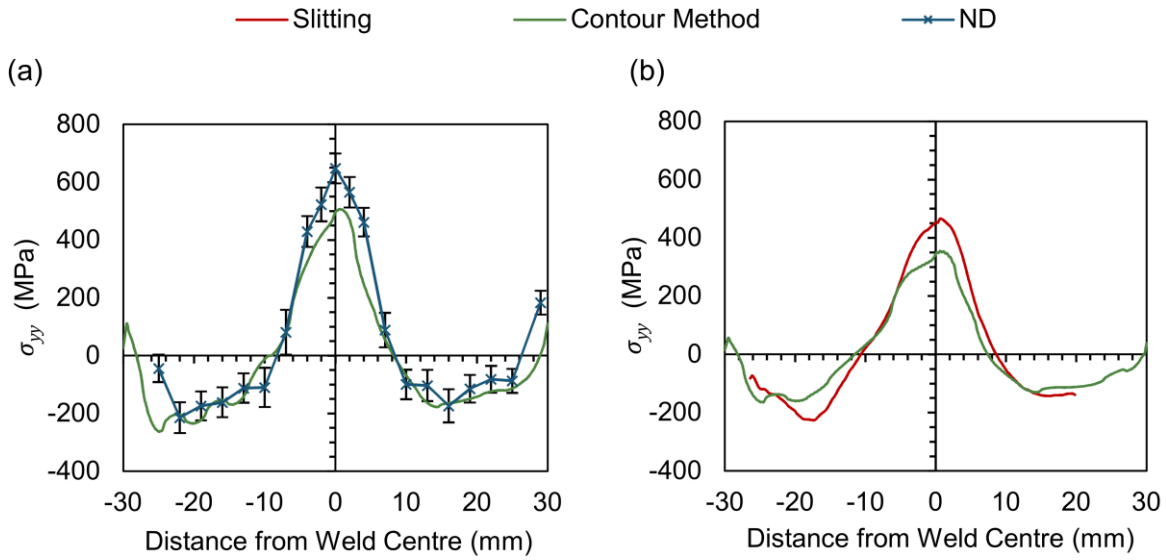

Figure 26 Comparison of longitudinal weld residual stresses in C(T) blank made from EBW4 using different measurement techniques (a) at mid-thickness and (b) averaged across thickness